REVIEW

Utilization of LDH-based materials as potential adsorbents and photocatalysts for the decontamination of dyes wastewater: a review

Zhongzhu Yang,[ab] Fenghua Wang,*[c] Chang Zhang,*[ab] Guangming Zeng,[ab] Xiaofei Tan,[ab] Zhigang Yu,[ab] Yu Zhong,[ab] Hou Wang[ab] and Fang Cui[ab]

Dye as a colored organic pollution has caused tremendous environmental problems. Removing dyes from effluents is of significant importance. Layered double hydroxides (LDHs), known as hydrotalcite-like compounds or ionic lamellar compounds, have attracted considerable attention recently due to the presence of large interlayer spaces, positively charged layers and solvation molecules. LDH-based materials are frequently used for environmental remediation especially for the elimination of dye compounds. This review compiles an extensive list of LDH-based low-cost sorbents and photocatalytic catalysts for dyes from the vast literature. Furthermore, performance, key factors and mechanisms involved in the processes are also included. Lastly, some major challenges together with prospects in this research field are discussed and highlighted. In conclusion, the application of LDH-based materials in the area of adsorption and catalysis science represents a useful and viable method, resulting in the outstanding capabilities in the removal of dyes from aqueous systems.

1. Introduction

Nowadays, the water pollution of organic dyes resulting from paper-made, dyeing, and other industries effluent has attracted global concern because of its significant impact on public health.[1] Besides the obvious aesthetic consequences, dyestuff

[a]*College of Environmental Science and Engineering, Hunan University, Changsha 410082, China. E-mail: 952157786@qq.com; zhangchang@hnu.edu.cn; Fax: +86-731-88822312; Tel: +86-731-88822312*

[b]*Key Laboratory of Environmental Biology and Pollution Control (Hunan University), Ministry of Education, Changsha 410082, China*

[c]*Institute of Physical Education, Xinjiang Normal University, Urumqi 830054, China*

discharges increase the biotoxicity and carcinogenic effects.[2,3] Furthermore, dyes are usually poorly biodegradable or recalcitrant to environmental conditions because of their complex structure and xenobiotic properties. Hence, color removal from dye effluents is one of the several major environmental concerns. Several methods have been developed for the remediation of wastewater containing dyes, including coagulation,[4] biological treatment,[5] ion exchange,[6] filtration,[7] adsorption[8] or photocatalysis.[9] Among these approaches, adsorption and photocatalysis have been widely used and proved to be reliable and capable of removing dyestuffs from wastewater.[10–15]

Adsorption offers flexibility in design and operation, in many cases it will generate high-quality treated effluent. In addition,

Zhongzhu Yang received his bachelor's degree of environmental engineering from Hunan University of Science and Technology. Now he is studying for a PhD degree at Hunan University. His research interests focus on clay-based materials, novel photocatalysts and adsorption materials for environmental applications.

Fenghua Wang received her doctor's degree of analytical chemistry from Hunan University. Then she worked in Hunan Normal University as a post-doctor. Her research interests are in biochemistry and analytical chemistry.

owing to the reversible nature of most adsorption processes, the adsorbents can be regenerated by suitable desorption processes for multiple use. Adsorption is hence recognized as the most versatile process used in lesser developing countries and is currently being used extensively for the removal of organic pollutants from the aqueous media.[16,17] Recently, many conventional sorbents have been used to remove dyes from wastewater, such as activated carbon,[18] bentonite,[19] and metal oxides,[20] fly ash[21] and coal.[22] However the main obstacles of these adsorbent materials are the relatively low adsorption capacity and the difficulty to reuse. The search for better efficiency and less-cost adsorbents seems unceasing.[23] At the meantime, photocatalysis which utilizes renewable solar energy to activate the chemical reactions *via* oxidation and reduction is a sustainable technology to provide solution for environmental issue. This photocatalysis system has attracted great interests from science community as the most promising way to solve the environmental problems, especially getting rid of residual dyes pollutants from wastewater stream.[24,25] This technique is based on the band theory and the n-type semiconductor is used as the photosensitized material, which is mainly metal oxide or metal sulfide. TiO_2, for example, is one of the most widely used photocatalyst, based on its good properties like chemically inert,

non-toxic to organisms, well-resourced, high energy gap.[26,27] But the industrial application is constricted by its low specific surface area, low surface adsorption rate and difficulty in recycling.[28] Developing recyclable semiconductor material which has a high quantum yield and visible light absorption rate is of great importance for the photocatalysis field.

Layered double hydroxides (LDHs), which are referred to anionic clays in comparison with cationic clays and also as hydrotalcite-like compounds (HT) are an important class of ionic lamellar solids. Layered double hydroxides (LDHs) with the general formula $[M_{1-x}^{2+}M_x^{3+}(OH)_2(A^{n-})_{x/n}]^{x+} \cdot mH_2O$, where M^{2+} and M^{3+} are divalent (*e.g.*, Mg^{2+}, Co^{2+}, Ni^{2+}, Zn^{2+}, Cu^{2+}) and trivalent cations (*e.g.*, Al^{3+}, Fe^{3+}, Ga^{3+}), respectively; x, ranging from 0.20 to 0.33, stands for the molar fraction of M^{3+} in the metallic ions; and A^{n-} is interlayer gallery anion (*e.g.*, CO_3^{2-}, Cl^-, NO_3^-, SO_4^{2-}). The excessive positive charges are balanced by intercalated hydrated anions in the inter-lamellar domain. The cation composition of the hydroxide layers, their charge density given by a M^{2+}/M^{3+} molar ratio, as well as interlayer anion composition can be tailored during LDH synthesis.[29–31] The structure of LDHs and a typical octahedral unit are shown in Fig. 1. By heating to 450–500 °C, LDHs can be converted into mixed metal oxides (MMOs), which exhibit fine dispersion of metal cations and high surface area. An important property of MMOs is the so-called "memory effect", that is the calcined anionic clays can reconstruct their original layered structure after adsorption of various anions.[32,33]

A set of characterization was performed to get better insight into the structural properties of LDH based materials. Typical XRD patterns of LDHs and CLDHs both before and after sorption experiments are shown in Fig. 2. A series of sharp (00*l*) peaks indexed as (003), (006), and (009) appearing as symmetric lines at low 2θ angle correspond to the basal spacing, indicating the presence of an ordered stacking sequence. The basal spacing of LDHs can be calculated based on the XRD results. After the adsorption, the XRD patterns of the recovered LDHs (Fig. 2b) are almost unchanged compared with the original LDHs (Fig. 2a), but their basal spacing may be different. The

Chang Zhang received his PhD degree at Hunan University. He ever worked as a as visiting scholar of Stanford University. He is an associate professor and doctoral supervisor in Hunan University now. His research interests are in remediation of water environment and water pollution control techniques.

Guangming Zeng received his PhD from Wuhan University in 1988. Later, he worked at the College of Environmental Science and Engineering, Hunan University. Now he is a professor at the Hunan University and also the director of Environmental Science and Engineering. His research interests include biosensor and bioimaging, especially fluorescence imaging in biological system based on QDs. After years of efforts, he has been rewarded many prizes and cultivated hundreds of master degree candidate and doctoral candidate.

Zhigang Yu received his Master's degree of environmental engineering from Hunan University. His research interest lies in pollutant removal from sediment and water, and also the synthesis of nanomaterials as adsorbents and photocatalysts in contaminated water.
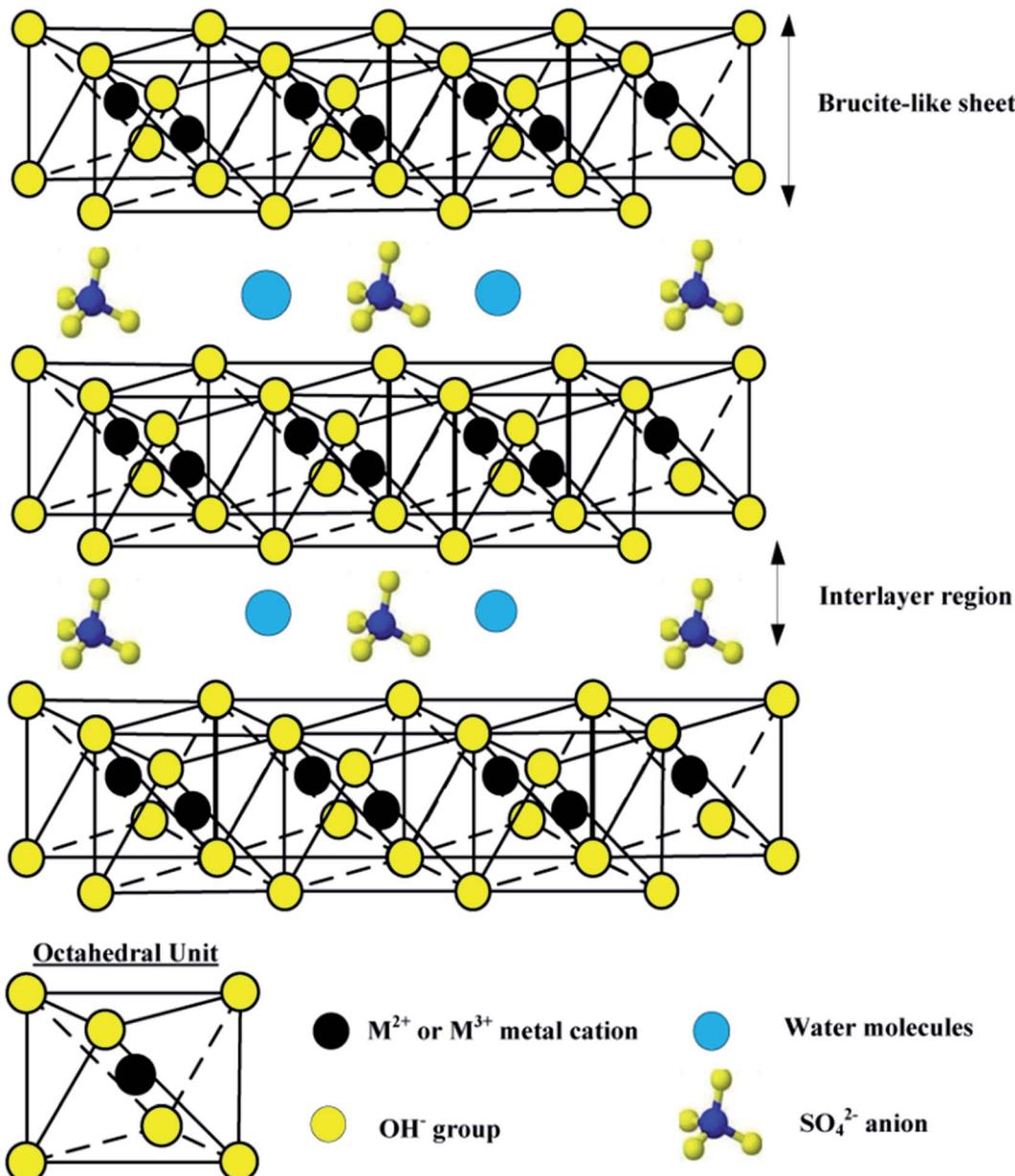
Fig. 1 The structure of a layered double hydroxide, with interlayer SO_4^{2-} anions.

interlayer spacing is always dependent on the size and orientation of the charge-balancing anion. The XRD pattern of CLDHs (Fig. 2d) shows that layered structure of the original LDHs is completely destroyed. The similar peak positions of the synthesized LDH and CLDH imply that the layered structure of LDH can be maintained after dyes sorption by CLDHs.[34] The morphology of the as-prepared adsorbent was observed by SEM and TEM. Fig. 3 shows the typical SEM image and TEM image of the LDHs. SEM image proves that the pure LDH has a hexagon structure and overlapping crystals.[35] As illustrated in Fig. 3, TEM image shows that the LDHs are smooth, well-shaped in hexagonal form, and overlapping crystals.[36]

LDHs have been used as adsorbents or anion-exchangers for the removal of various anionic species in aqueous solutions, because these compounds present properties such as a layered structure, high porosity, high surface area, and interlayer anion mobility.[37] Our previous research has demonstrated that the Fe–Al LDH is capable for the reduction of bromate in solution.[38] Besides the excellent efficiency the field of adsorption, the photo-decomposition performance of dyes was found on LDHs composed of various metals such as Ni, Zn, and Cr. It resulted from the well distribution of metals in the hierarchical structure, because that doping or composition would enhance the dye sorption inside the particle and also high light absorption in the spectral range.[11,28,39] Indeed, increasing interest has been diverted to evaluating the ability of LDHs to remove dyes from aqueous solutions by the process of adsorption and photocatalytic degradation. This is because LDHs have exhibited
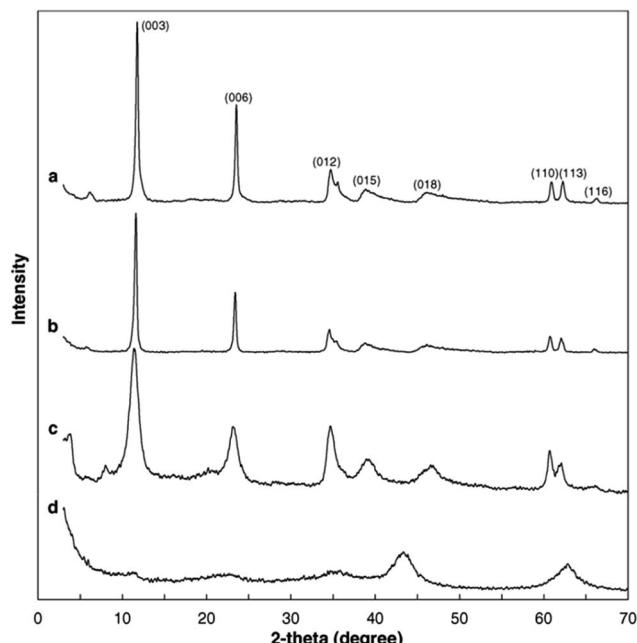
Fig. 2 X-ray diffractograms of layered double hydroxides (LDHs) and calcined LDHs (CLDHs) before and after Brilliant Blue R (BBR) sorption. (a) LDHs; (b) LDHs after BBR sorption; (c) CLDHs after BBR sorption; (d) CLDHs (adapted from ref. 34 with Copyright from 2005 Elsevier).

a great potential to efficiently remove harmful dyes due to their superior characteristics as mentioned in the preceding discussion.

Although the existence of reviews highlights dyes removal from aqueous solution by adsorption[40,41] and the application of LDH-based materials in the area of environmental remediation,[31,42,43] there is no review article describes the use of LDH materials in the removal of dyes. This review introduces briefly the use of LDH materials as adsorbents and catalysts in the decontaminant of dyes. We addressed the complexity of the many factors that influence the adsorption process as well as mechanisms. Besides we also examine various LDHs based materials used as photocatalysis that are capable of degrading

dyes, and describe their performance, characteristics, advantages and limitations. Finally, challenges and outlook are put forward to facilitate exciting developments in this promising area in the future.

2. Adsorption of dyes on LDHs

The high anion exchange capacity and large surface area of LDHs, their flexible interlayer region that is accessible to various ionic and non-ionic compounds are important characteristics promising their better removal performance of contaminants from aqueous system. Thus far, various dyes including anionic dyes, cationic dyes, and non-ionic dyes are investigated. Fig. 4 shows a process flow diagram of LDH preparation from coprecipitation method and batch adsorption process for dye removal. The summaries of LDHs that have been used to treat various dyes along with their adsorption capacity of each are presented in Tables 1 and 2. It was clearly that dye sorption was influenced by pH, temperature and various functional groups presented on LDHs. Here we have outlined the above mentioned factors that influenced the dyes removal process.

2.1. Adsorption isotherms and capacities

Adsorption equilibrium is one of the crucial pieces of information needed for the proper analysis and the isotherm indicates how the molecules distribute between the liquid and solid phase when reaching the equilibrium state. Besides, isotherms help to provide information about the optimum use of adsorbents.[92] A number of empirical models have been employed to analyze experimental data and describe how adsorbates interact with adsorbents. The Langmuir and Freundlich isotherms are the most frequently used to examine the adsorption date of dyes adsorption onto LDHs. The Langmuir model is based on the assumptions that all the adsorption sites are equivalent, and the adsorption occurs in a monolayer form without any interactions between adsorbed molecules,[93] while the Freundlich isotherm assumes the heterogeneous surfaces and is known to be satisfactory for low concentrations.[94]
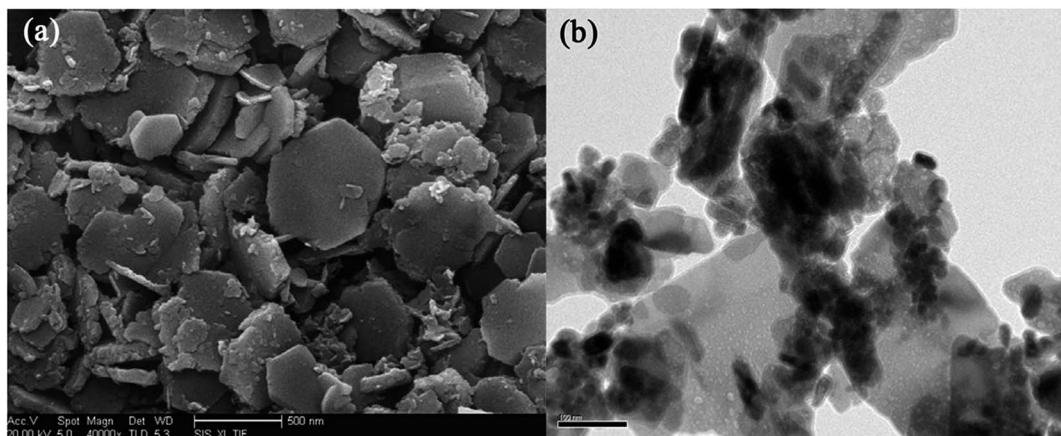
Fig. 3 SEM images (a) and TEM images (b) of Zn−Al LDH (image (a) adapted from ref. 35 with Copyright from 2014 Elsevier and image (b) adapted form ref. 44 with copyright from 2016 Elsevier).
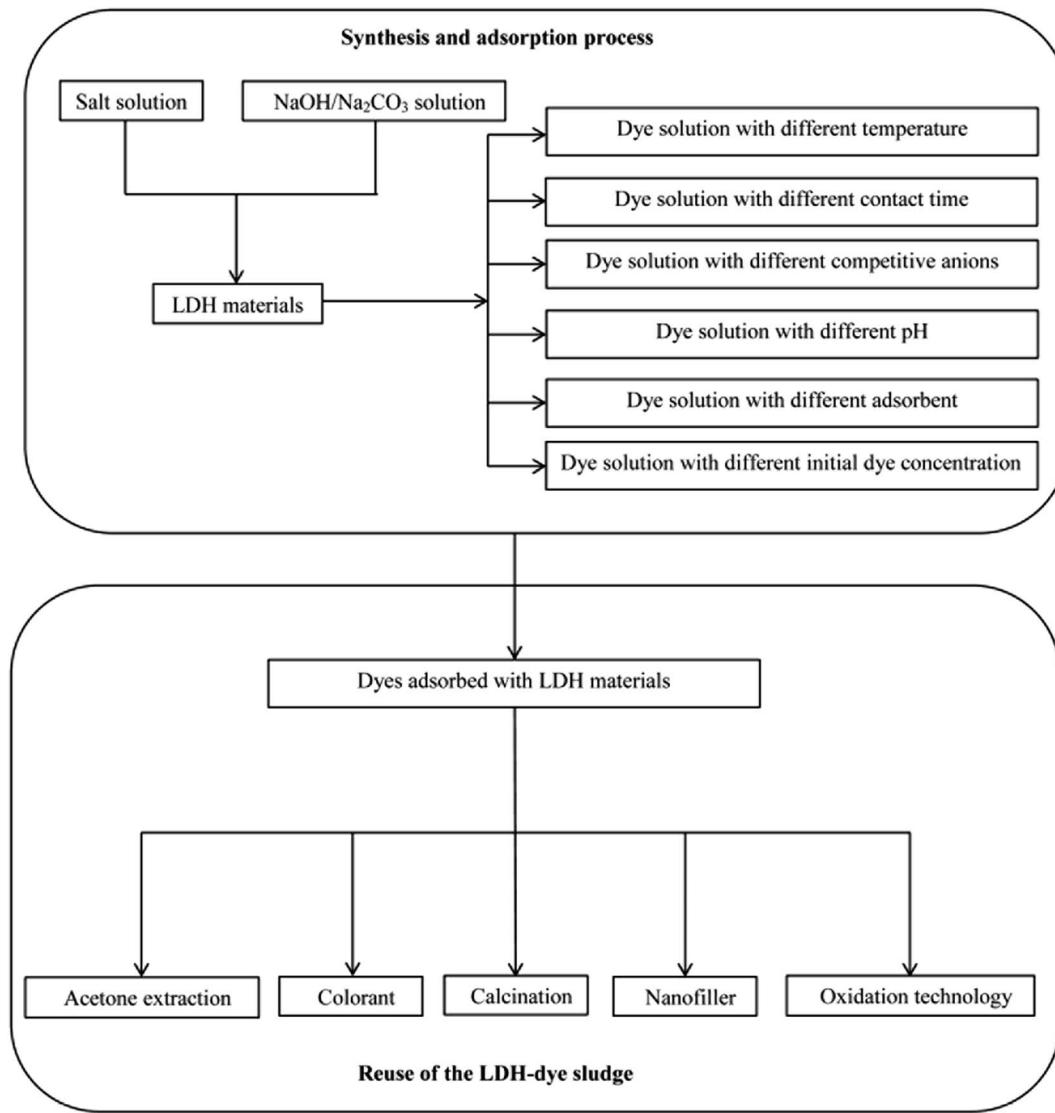
Fig. 4 Schematic diagram of the system for various dyes removal and reuse of the LDH–dye sludge.

2.1.1. Adsorption isotherms and capacities of uncalcined LDHs. The common adsorption isotherms employed to represent equilibrium uncalcined LDHs-dyes date follow the order Langmuir > Freundlich just as shown in Table 1. This indicates that the LDHs material forms a monolayer on surface with a finite number of identical sites and there is no interaction between adsorbed molecules. It is notable that most of the studies used the linear form for Langmuir equation to fit observed data. Lafi *et al.*[45] studied adsorption isotherms of CR adsorption onto the Mg–Al LDH at different initial concentrations. The correlation coefficients suggested that the Langmuir model ($R^2 = 0.993$) fitted the data better than the Freundlich model ($R^2 = 0.88$). The results of adsorption experiments indicated that the maximum capacity of CR was found to be 111.11 mg g^{-1}. Application of the Freundlich isotherm reveals information regarding the chemisorption mechanisms that govern the equilibrium, but only a few studies have showed the Freundlich isotherm is better to model the adsorption

equilibrium between target dyes pollutants and LDHs. In the adsorption of CR onto Mg–Fe LDH, adsorption isotherms were simulated with Langmuir and Freundlich equations, a correct fit for Langmuir model was observed but Freundlich model fitted better and the saturated adsorption capacity of Mg–Fe LDH for CR was found to be 104.6 mg g^{-1}.[95]

2.1.2. Adsorption isotherms and capacities of calcined LDHs. As evidenced by the data shown in Table 2, the Langmuir model fits the adsorption data of dyes onto calcined LDHs in most cases. Benselka-Hadj Abdelkader *et al.*[79] studied Orange G dye adsorption onto the calcined Mg–Fe LDH adsorption isotherms at different initial concentrations and found that the Langmuir model ($R^2 = 0.9959$) fit the data better than the Freundlich model ($R^2 = 0.9504$). Ni *et al.*[88] investigated the MO adsorption by calcined Zn–Al LDH, a correct fit for Langmuir model was observed but Freundlich model fitted better. In addition to the popular Langmuir and Freundlich isotherm models, Redlich–Peterson isotherm model has also been used

Table 1 Adsorption capacities and experimental conditions of uncalcined LDHs for the removal from aqueous solutions

LDHs	Synthesis	Dyes	Optimum pH	Nature of adsorption	Adsorption capacity (mg g^{-1})	Kinetic model	Isotherm	Ref.
Mg–Al LDH	Coprecipitation	Congo red	—	Endothermic	111.111	2nd	L	45
Mg–Al LDH	Hydrothermal	Methyl orange	4	—	329.27	2nd	F	10
Mg–Al LDH	Coprecipitation	RR, CR, AR 1	—	—	59.49, 37.16, 108	2nd	L	46
Mg–Al LDH	Coprecipitation	MO, OII, OG	—	Exothermic	1800, 1189, 769	2nd	—	47
Mg–Al LDH	Colloidal deposition	Methylene blue	—	—	185	2nd	L	48
Mg–AL LDH	Coprecipitation	Brilliant red K-2BP	4	Endothermic	657.5	2nd	L	49
Mg–AL LDH	—	Acid blue 113	—	—	47	2nd	L	50
Mg–AL LDH	Coprecipitation	Benzopurpurin 4B	—	Endothermic	153.88	—	—	51
Mg–Al LDH	Coprecipitation	Acid blue 9	—	—	59.5	—	L	52
Mg–Al LDH	Coprecipitation	Acid green 68:1	—	—	99.1	2nd	L	53
Mg–Al LDH	Coprecipitation	Reactive red	2–10	—	59.49	2nd	L	54
Mg–Al LDH	Coprecipitation	Congo red	4	—	37.16	2nd	L	54
Mg–Al LDH	Coprecipitation	Acid red 1	9	—	108	2nd	L	54
Mg$_2$–Al LDH	Coprecipitation	Orange II	—	Endothermic	1265	—	L	55
Mg–AL LDH	Coprecipitation	Green bezanyl-F2B	5–9	—	52.08	2nd	L	56
Mg–Fe LDH	Coprecipitation	Yellow GX	—	Endothermic	53.76	2nd	L	57
Mg–Ni–Al LDH	Coprecipitation	Methyl orange	6–9	Endothermic	118.5	2nd	L	58
Ca–Al LDH	Coprecipitation	Sunset yellow FCF	4	—	398.41	—	L	59
Ni–Fe LDH	Hydrothermal	Evans blue	—	—	—	—	—	60
Ni–Al LDH	Coprecipitation	Brilliant red X-3B	—	Exothermic	48	2nd	L	61
Ni–Zn–Cr LDH	Accelerated carbonation	Acid scarlet GR	5	—	122	I-P	L	62
Cu–Al LDH	Coprecipitation	Methyl violet 2B	—	—	361	2nd	L	63
Zn–Al LDH	Stepwise growth	Methyl orange	—	—	523	—	—	64
Zn$_2$–Al LDH	Coprecipitation	Acid red 97	—	—	299.5	2nd	—	65
Zn$_2$–Al LDH	Coprecipitation	Evans blue	—	Endothermic	491.93	—	L	66
Zn$_2$–Al LDH	Coprecipitation	Chicago blue sky	—	Endothermic	501.36	—	L	66
Zn$_2$–Al LDH	Coprecipitation	Niagara blue	—	Endothermic	536.13	—	L	66
Zn$_3$–Al LDH	Coprecipitation	Methyl orange	—	—	—	—	F	67
Zn$_3$–Al LDH	Coprecipitation	Fast green	—	—	51.24	—	F	67
Zn–Mg–Al LDH	Coprecipitation	Methyl orange	3	—	883.24	2nd	L	68
HB–Zn–Al LDH	Coprecipitation	Methylene blue	4	—	30.87	2nd	L	69
Fe$_3$O$_4$–Zn–Cr LDH	Hydrothermal	Methyl orange	6.4–7.3	—	240.16	2nd	—	70
Fe$_3$O$_4$–Zn–Cr LDH	Hydrothermal	Methyl orange	—	—	528	—	L	71
DA–Mg–Al LDH	Coprecipitation	Methyl orange	3	Exothermic	—	2nd	—	72
ILs–Mg–Al LDH	Coprecipitation	Reactive orange 5	—	Endothermic	300.9	2nd	F	73
DGLN–Mg–Al LDH	Coprecipitation	Victorial blue B	—	—	1064	—	L	74
DGLN–Mg–Al LDH	Coprecipitation	Weak acidic green GS	—	—	131	—	L	74
DGLN–Mg–Al LDH	Coprecipitation	Ethyl violet	—	—	415	—	L	74
SDS–Mg–Al LDH	Self assembly	Disperse violet 28	—	—	—	2nd	Linear	75
SDBS–Mg–AL LDH	Coprecipitation	Safranin	5–8	—	40.5	2nd	L	76
SDS–Mg–AL LDH	Coprecipitation	Safranin	5–8	—	83.3	2nd	L	76
SDS–Mg–AL LDH	Calcination rehydration	Green bezanyl-F2B	5–9	—	188.68	2nd	L	56
SDS–Mg–Al LDH	Coprecipitation	Direct blue G-RB	5–10	Endothermic	707.76	2nd	L	77
SDS–Mg–Al LDH	Coprecipitation	Yellow 4 GL	5–10	Endothermic	392.88	2nd	L	77
SDS–Mg–Al LDH	Coprecipitation	Acid red GR	5–10	Endothermic	137.33	2nd	F	77
SDS–Mg–Al LDH	Coprecipitation	Disperse red 3B	5–10	Endothermic	249.24	2nd	L	77
SDS–Mg–Al LDH	Coprecipitation	Basic blue	5–10	Endothermic	165.11	2nd	L	77

to examine the adsorption equilibrium data of dyes adsorption onto calcined LDHs. For example, the adsorption data of MO adsorbed on calcined GO–Ni–Al LDHs was found to be fitted better to the Redlich–Peterson model with a R^2 value of 0.9831 higher than Langmuir model ($R^2 = 0.9770$) and Freundlich model ($R^2 = 0.9058$).[91] As another example, Zhang et al.[89] synthesized MnO$_x$ modified Zn–Al LDO as adsorbent for the removal of MO, the adsorption equilibrium data was best represented by the Redlich–Peterson isotherm. These results

revealed that the MO adsorption on calcined GO–Ni–Al LDHs and MnO$_x$–Zn–Al LDO were not an ideal monolayer adsorption. However, the isotherms are unable to definitively illustrate the sorption mechanism. One cannot differentiate between precipitation and sorption by the adsorption isotherm.[96] The mechanism should be illustrated by various characterization methods.

The adsorption capacities of calcined LDHs for various dyes in aqueous system are also summarized in Table 2. It is evident that

Table 2 Adsorption capacities and experimental conditions of calcined LDHs for the removal from aqueous solutions

LDHs	Synthesis	Dyes	Optimum pH	Nature of adsorption	Adsorption capacity (mg g^{-1})	Kinetic model	Isotherm	Ref.
C–Mg–Fe LDH	Coprecipitation	Methyl orange	—	Exothermic	194.9	2nd	L	78
C–Mg–Fe LDH	Coprecipitation	Acid brown 14	4–11	—	370.0	2nd	L	33
C–Mg–Fe LDH	Coprecipitation	Orange G	3–13	Endothermic	378.8	2nd	L	79
C–Mg–AL LDH	Coprecipitation	C.I. acid blue 9	—	—	194.48	—	L	80
C–Mg–Al LDH	Opal inverse	Orange II	—	—	1550.5	—	L	81
C–Mg–AL LDH	—	Acid blue 113	—	—	2544	Avrami's	L	50
C–Mg–AL LDH	Coprecipitation	Acid blue 29	—	—	36	—	L	82
C–Mg–AL LDH	Coprecipitation	Indigo carmine	5–9	—	1343	—	F	32
C–Mg–AL LDH	Coprecipitation	Remazol red 3BS	6	Endothermic	134.4	2nd	L	83
C–Mg–AL LDH	Coprecipitation	Acid green 68:1	3–10	—	154.8	2nd	L	53
C–Mg–AL LDH	Coprecipitation	Brilliant blue R	3.5–13	—	615	2nd	F	34
C–Mg–AL LDH	Coprecipitation	Benzopurpurin 4B	—	Endothermic	417.36	—	—	51
C–Mg–Al LDH	Coprecipitation	Acid red G	10	Exothermic	93.1	—	—	84
C–Mg–Al LDH	Coprecipitation	Acid orange 10	4	Endothermic	665	2nd	L	85
C–Mg–Ni–Al LDH	Coprecipitation	Methyl orange	6–9	Endothermic	375.4	2nd	L	58
C–Ni–Al LDH	Coprecipitation	Remazol brilliant violet	6	—	150	—	—	86
C–Zn–Al LDH	Hydrothermal	Methyl orange		—	—	2nd	L	87
C–Zn–AL LDH	Coprecipitation	Methyl orange	6	Endothermic	181.9	2nd	F	88
C–MnO$_x$–Zn–Al LDH	Intercalation reduction	Methyl orange	—	Endothermic	617.28	2nd	R–P	89
C–Au–Zn–Al LDH	Coprecipitation	Methyl orange	—	—	627.51	—	L	90
C–GO–Ni–Al LDH	Hydrothermal	Methyl orange	—	—	210.8	2nd	R–P	91

the calcined sample exhibited better removal efficiency compared with its parent hydrotalcite. At a similar BBR equilibrium concentration of 100 mg L^{-1}, sorption capacity of calcined LDHs was more than 10 times greater than that of LDHs.[34] In another adsorption experiment, calcined and non-calcined LDHs were used as adsorbents to remove azo dye acid green 68:1 in an aqueous solution. The results indicated that calcined Mg–Al LDH possesses greater adsorption capacity (154.8 mg g^{-1}) than non-calcined Mg–Al LDH (99.1 mg g^{-1}). The larger sorption capacity of CLDH than that of LDH can be attributed to their property of structural reconstruction, higher surface area, the presence of stronger basic sites and anion exchange.[33,53]

2.2. Adsorption kinetics

The calculated kinetic parameters can be of a great practical value for technological applications. Many studies used kinetic models to study the fast changing kinetic data to estimate the sorption rates and to determine the possible controlling mechanism and the potential rate-limiting steps.[97] In most experiments the amounts of sorbed dyes increased rapidly within the initial time and remained almost unchanged after complete equilibrium. Among the models to study the adsorption of dyes using LDHs materials: (1) the pseudo-first-order kinetic model; (2) the pseudo-second-order kinetic model; and (3) the intra-particle diffusion model are the three most widely used. The assumption of the pseudo-first-order model was physical adsorption and the solute uptake rate with time is directly proportional to ratio of the solute concentration and the amount of solid, while the pseudo-second-order kinetic model is based on the assumption that the rate-limiting step may be chemical adsorption or chemisorption involving valence forces

through sharing or exchange of electrons between adsorbent and adsorbate.[98]

2.2.1. **Adsorption kinetics of uncalcined LDHs.** Seen from the Table 1, the pseudo-second-order kinetic models fitted almost all the process of dyes adsorbed onto uncalcined. For instance, Zheng et al.[68] synthesized nanostructured microspheres of applied the pseudo-first-order kinetic model and the pseudo-second-order kinetic mode to investigate the kinetics date for MO adsorption by using Zn–Mg–Al LDH at four different initial concentrations (0.05 g L^{-1}, 0.1 g L^{-1}, 0.125 g L^{-1}, 0.25 g L^{-1}). The results showed that the reaction followed the pseudo-second-order kinetic model much better. In another study of MO adsorption by Fe$_3$O$_4$–Zn–Cr LDH, a similar results, the pseudo-second-order kinetic model fitted the date.[70] For the adsorption of RY on SDS–LDH, the adsorption process was fairly fast, reaching equilibrium after 30 min. The fast removal rate at the beginning was attributed to the rapid diffusion from solution to the external surfaces. The sequent slow process was due to the longer diffusion range to the internal surfaces or reaction.[99]

Besides the surface adsorption, intraparticle diffusion or pore diffusion plays a key role, and therefore the rate-limiting step may be involved in film and/or pore diffusion. To determine if the rate limiting step is intraparticle diffusion or not, some researchers applied the Weber–Morris model diffusion law. In the removal of CR by Mg–Fe LDH, the effect of intra particle diffusion resistance on adsorption was evaluated and results showed that intra particle diffusion had a significant role in the adsorption.[95]

2.2.2. **Adsorption kinetics of calcined LDHs.** It is also evident from Table 2 that the pseudo-second-order kinetic models fitted almost all the process of dyes adsorbed onto

calcined LDHs. For example, both Mg–Ni–Al LDH and calcined Mg–Ni–Al LDH were used in the adsorption of MO from aqueous solution and the dynamical data fitted well with the pseudo-second-order kinetic model.[58] However, the kinetic profiles were different in the uptake of the acid blue 113 by hydrotalcite and calcined hydrotalcite. The uptake rate by Mg–Al LDH was described by the pseudo-second order adsorption model, whereas sorption by calcined Mg–Al LDH fitted the Avrami's equation. Dye intercalation during reconstruction of the laminar structure must involve nucleation and growth. Thus, the Avrami's equation must be more suited to describe the rate of dye removal by calcined LDH than simple adsorption kinetic schemes.[50] To identify the diffusion mechanism in the adsorption of AB 14 on calcined Mg–Fe LDH, intraparticle mass transfer diffusion model proposed by Weber and Morris was used. It was found that the q_t versus $t^{1/2}$ was not linear, which indicated the intra-particle diffusion was not the rate-limiting step of the adsorption process.[33]

It is noted that pseudo-second-order model well fitted to the kinetic data for all the studied process rather than pseudo-first order (Tables 1 and 2). This demonstrates that the rate-limiting step in the adsorption involves chemisorption due to valence forces through the sharing or exchange of electrons between sorbent and sorbate, complexation, coordination, and/or chelation.[100] The mechanism of dyes sorption by LDHs is complex and probably involves a combination of external mass transfer and intraparticle diffusion through the macropores/micropores of LDHs.

2.3. Factors affecting adsorption of dyes on LDHs

Optimisation of aqueous conditions will greatly help the development of industrial-scale dye removal treatment process. There are seven factors that influence the dyes removal, as mentioned in the following sector.

2.3.1. Effect of temperature.
Temperature can influence the mobility of dyes, the solubility of dyes and change the equilibrium capacity. From Tables 1 and 2, it was observed that most of the reactions are endothermic which indicated that the adsorption is favored at higher temperature. This may be due to increasing mobility of the dye molecules and an increase in the number of active sites for the adsorption with increasing temperature. The AB 14 dye onto calcined Mg–Fe LDH was reported as an endothermic process. Adsorption capacity increased from 130 mg g^{-1} to 540 mg g^{-1} with increase in temperature from 283 K to 323 K.[33] Similar trend was observed in the process of RBR K-2BP adsorption by Mg–Al LDH, the capacity increased with increase in temperature from 293 K to 323 K. The Gibbs free energy change ($\Delta G°$) was negative and enthalpy change ($\Delta H°$) was positive, so the adsorption process was spontaneous and endothermic. The positive entropy ($\Delta S°$) change may be due to the release of water molecules and the chloride anions from the MMH ion exchange.[49]

Apart from the endothermic adsorption process, several studies reported on adsorption process are of exothermic in nature. For example, adsorption of MO, OII and OG on fresh Mg–Al LDH, and direct calorimetry measurements of the enthalpy change accompanying the dye retention by LDH were carried out to demonstrate the exothermic character of the overall mechanism.[47] The other example was the uptakes of MO onto DA–Mg–Al LDH decreased with an increase of temperature, which reflected that LDH may be unstable at high temperature.[72] Tong et al.[84] studied the effect of temperature on adsorption of ARG onto calcined Mg–Al LDH from 298 K to 338 K and found the adsorption slightly decreased with increasing temperature, which indicated that the lower temperature favored the adsorption of ARG and it was an exothermic process.

2.3.2. Dosage of adsorbent.
An optimum dosage is crucial for a cost-effective system. The effect of adsorbent dosage on the adsorption process can be carried out by prepare adsorbent–adsorbate solution with different amount of adsorbents added to fixed initial dye concentration then shaken together until equilibrium time.[101] Usually, the removal ratio of dye increases with the increasing amount of calcined LDH and uncalcined LDH. The removal rate of AB 14 increased sharply with the increment of the adsorbent dosage, and when a 50 mg L^{-1} AB 14 solution was treated by using 0.2 g L^{-1} calcined LDH, the removal percentage reached almost 100%. The effect of fresh Mg–Al LDH and calcined Mg–Al LDH dosages on the AB 14 adsorption are shown in Fig. 5. The calcined material showed much higher adsorption ability than that of the fresh LDH material.[33] In another study, removal percentage of BBR adsorbed increased almost linearly with increasing dosage of calcined LDH before a complete removal of BBR, probably implying that the amount of sorption sites also increased linearly with increasing dosage during structural reconstruction.[34]

The percentage removal of MO increased from 39% to 96% when the adsorbent dosage increased from 0.2 to 10 g L^{-1}. This was probably due to the low adsorbent dosage that causes the dispersion of LDHs grains in aqueous solution, therefore all types of sites on the adsorbent surface were entirely exposed which will facilitate the accessibility of MO molecules to a large
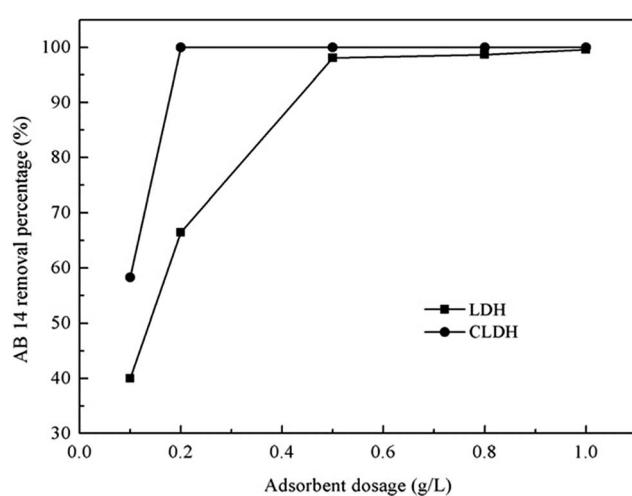
Fig. 5 Effect of adsorbent dosages on the removal of AB 14 by Mg–Al LDH and calcined Mg–Al LDH (adapted from ref. 33 with Copyright from 2013 Elsevier).

number of sites. In this case, the adsorption on the surface was saturated quickly, showing a high uptake capacity. Lower adsorption capacity of the calcined Mg–Al–Ni LDHs was, however, obtained with the higher adsorbent dose. Because at higher particle concentrations the availability of sites with higher energy decreased with a larger fraction of sites with lower energy becoming occupied, leading to a lower adsorption capacity. Besides, higher adsorbent amount enhanced the probability of collision between solid particles and therefore created particle aggregation, causing a decrease in the total surface area and an increase in diffusion path length, both of which contribute to the decrease in the adsorption capacity.[58] However, the OG amount adsorbed by both LDH and CLDH increased with increasing sorbent dose until 1.4 g L^{-1}, from this dose the quantities of dye adsorbed on both materials were still unchanged. This may be explained by the good dispersion of materials particles on OG solutions, where the adsorbed and exchanged sites of materials were probably more open.[79] These controversial findings highlight the needs for a comprehensive investigation of the material property in order for cost-effective application.

2.3.3. Effect of pH. It is postulated that the pH value of the solution is an important parameter for the adsorption process, which influences the structure and the surface properties of adsorbents.[102] The effect of solution pH is an important factor affecting not only the surface charge of LDHs, but also the degree of ionization of the material, the dissociation of the functional groups on the active sites of LDHs and solubility of some dyes. Further the pH effect on the dye adsorption by LDHs is dependent on the type of dye and the type of LDHs. The optimum pH values obtained for various dye removal by LDHs were summarized in Tables 1 and 2.

The surface charge of LDH was positive when pH < pH$_{PZC}$ and negative when pH > pH$_{PZC}$. Theoretically, at pH < point of zero charge (PZC), the surface gets positively charged, which enhances the adsorption of the negatively charged dye anions through electrostatic forces of attraction. At pH > pH$_{PZC}$, the surface of LDHs particles gets negatively charged, which favors the adsorption of cationic dye.[103] Therefore, at a solution pH lower than pH$_{PZC}$, hydrogen ions were in the solution making the surface of the adsorbent with more positive charges, which promoted the electrostatic attraction between the negatively charged anion of the dye and the surface of the adsorbent. In contrast, the surface of the LDH may acquire negative charges at a solution pH higher than pH$_{PZC}$. The competitive effects of OH$^-$ ions and the electrostatic repulsion between the anionic dye molecules and the negatively charged active adsorption sites on the LDH would result in a decrease in the adsorption capacity.[10,104] For example, the adsorption of Sunset Yellow FCF food dye was favored at pH values near 4.0. Between pH 4.0 and 10.0, the adsorption of dye by Ca–Al LDH decreased with increasing solution pH. The authors reported that the decreased adsorption was due to the deprotonation and competition with the OH$^-$.[59] The effect of the pH value on the adsorption of MO on the uncalcined and calcined Mg–Ni–Al LDH were exampled. There was a decrease in MO adsorption when the equilibrium solution pH was less than 4 and greater

than 10, which was partially caused by the dissolution of LDHs.[58] Similar explanation was given for the adsorption of MO onto Zn–Al calcinated LDH, which the percentage of adsorption reached the maximum at pH 6.[88]

However, a few sorption cases were found to be independent of pH, this is probably because of the buffering properties of uncalcinated LDHs.[76,77,105] At low pH values, the hydroxyl groups in the LDH interlayers can neutralize the hydrogen ions in the solution, while at high pH values, the surface is deprotonated, and thus may have buffering effects on the hydrogen groups. These conditions also happened in the calcined LDH that the effect of initial pH over a wide pH range on the adsorption were minimal.[32–34,79] Effect of pH on BBR sorption at a fixed initial concentration and CLDH dosage is shown in Fig. 6. It may be concluded that the effect of initial pH over a wide pH range (3.5–13.0) on anionic dye removal by CLDHs is minimal. The reason was probably due to the reconstruction of the LDH structure with the intercalation of dye molecular into the CLDH[33] or OH$^-$ release[34] in aqueous solutions. It should be noted that, however, the effect of pH on both cationic and anionic dye sorption by many other adsorbents, for example, fly ash and acid-activated bentonite was pronounced.[106,107] This is an advantage of CLDH in relation to other types of adsorptive materials that usually show a large dependency on pH for adsorption.

The relationship between the initial and final pH for MO adsorption on Mg–Al LDH was checked. At low initial pH (pH$_i$), the final pH values (pH$_f$) were higher than pH$_i$ values, which was due to the protonation and/or the dissolution of LDH.[10] Fig. 6 also shows the difference between initial and final pH values. It can be seen that when initial pH values were lower than 10.0, final pH values can be enhanced and finally stabilized within a narrow alkaline range of 10.6–10.8. This is environmentally meaningful for precipitation or co-precipitation of some co-existing metal cations like Ca^{2+}, Pb^{2+} and Cd^{2+}.[34] The increase of the final pH value was observed and this is due to the proton consumption during the reconstruction process. Thus, the pH increase probably produces an increase of the negative surface
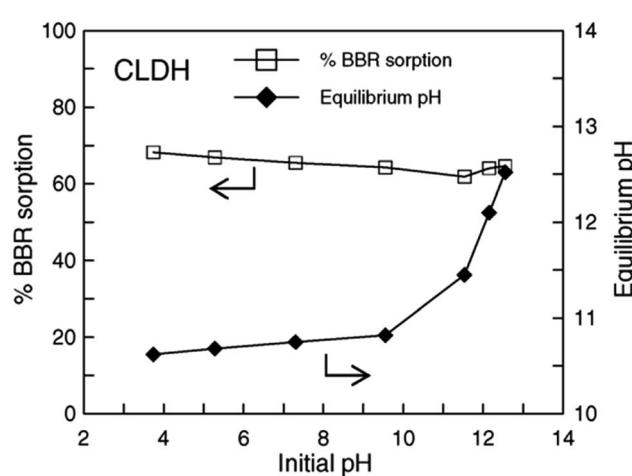

Fig. 6 Effect of initial pH on Brilliant Blue R (BBR) sorption by calcined layered double hydroxides (CLDHs) and on equilibrium pH (adapted from ref. 34 with Copyright from 2005 Elsevier).

charges and the interaction between the anion dye and the surface charges decrease.[85] At very low pH values, there are the possibility of dissolution and/or leaching of the CLDH. The dissolved material causes a fast increase in pH medium and consequently a decrease of the dissolution rate. Thus, the remaining adsorbent material is then responsible for the high adsorption capacity.[53,69,95] It should be mentioned that the decrease in uptake capacity with decreasing pH may be due to the structure of layered materials with hydroxide sheets was partial destroyed.[84,85,104] The discrepancies on the reported in lower pH influencing on adsorption may be due to the different dye molecule forms, dissociation constant[67,95] and different origins of the LDH samples.[50]

2.3.4. Effect of materials component. The nature of the LDH precursor metals, including different combinations of the metals, atomic ratio of the metals were studied in some cases. For example, the effect of Zn and Au content of the Au/Zn–Al LDO nanocomposites on sorption capacity was checked. It confirmed that the sample with Zn content of 87% was the most efficient one, because with the increasing Zn content the porous ZnO phase would be formed. By tailoring Au content (0–5%) in the composites, the sorption would reach the maximum with 1% of Au introduction, while varying Au content to the higher point (5%) and lower point (0.2%), the percentage removal of MO was lower than 60%, which resulted from the formation of Au aggregate with higher Au introduction (Fig. 7).[90] In another study of MO adsorption, the different molar ratio of Zn/Mg (0, 0.12, 0.5, 0.8) were checked, unexpectedly, adsorption capacity with Zn/Mg = 0 was even higher than samples with Zn/Mg = 0.5 and 0.8. This was because Mg–Al LDHs were homogeneous hexagonal platelets, which were favorable for MO to "stand" on the surface compared with the destroyed anthoid spheres.[68] The MO sorption were also influenced by layer charge, different adsorptive capacity of MO onto Zn–Al LDH resulted from the differences in their layer charge (that was, Zn_2Al–LDH > Zn_3Al–LDH > Zn_4Al–LDH). It was believed that anion adsorption can be enhanced by increasing the exchange capacity.[67]

For a given choice of metal cations and interlayer anions, the best crystalline LDH phase was generally obtained with an M^{2+}/M^{3+} ratio of 3 : 1.[108] In the removal of OG, various Mg/Fe molar ratios of 2–5 were prepared. As seen from XRD, the influence of Mg/Fe molar ratios was apparent and the good crystallinity was obtained when Mg/Fe molar ratio equals 3.[79] However, in the adsorption of AB 9, AY 23, and AR 37 onto Mg–Al LDH of variable Mg/Al molar ratio, the optimum molar ratio was reported to be 4.[109] The adsorption abilities of calcined and uncalcined Mg–Al LDH with different Mg/Al molar ratios were investigated to adsorb AB 9. The optimum adsorption of AB 9 was achieved by LDHs with Mg/Al molar ratios varying from 3.1 to 4.4. The highest pore volumes were measured for materials with the best dye affinity at Mg/Al molar ratios of 3.1 and 4.4. When Mg/Al molar ratio was above 4.4, the surface area started to decrease and so did the adsorptive capacity.[52] In the case of CLDH, initial dye affinity tests indicated particularly strong adsorption for materials with Mg/Al ratios of 3.1 to 7.6. At low initial Mg/Al, there would be less MgO in the CLDH product but with more Mg(Al)O mixed oxide phase that can be formed after calcination. This therefore can lead to less basic sites that may be responsible to less adsorption of AB 9.[80]

These observations collectively demonstrate that the nature and content percent of precursor metals have a significant impact on the adsorption due to the influence on crystallinity of the samples.

2.3.5. Effect of modification. The modification of LDH is attracting increasing interest in the scientific community as new and fascinating properties are being discovered with ligands introduction. The main objective of modification aims to enlarge their adsorption properties.

Considering the superior adsorption capacity of nanomaterials, a few nanomaterials based LDHs have been prepared to check the performance. Zhang et al.[90] synthesized Au/ZnAl–LDO nanocomposites through a facile calcination process of $HAuCl_4$ intercalated Zn–Al LDH nanocomposites. AuNPs with small size were well dispersed in calcined Zn–Al LDO matrix. The presence of AuNPs with smaller size, not only had the adsorption ability for MO, but could fabricate lot of porous channel in LDO matrix for the adsorption, resulting in a great high adsorption property. The percentage removal of MO from the solution was 98.99% compared to 48.18% without Au loading. In another study, ZnO nanorods decorated calcined
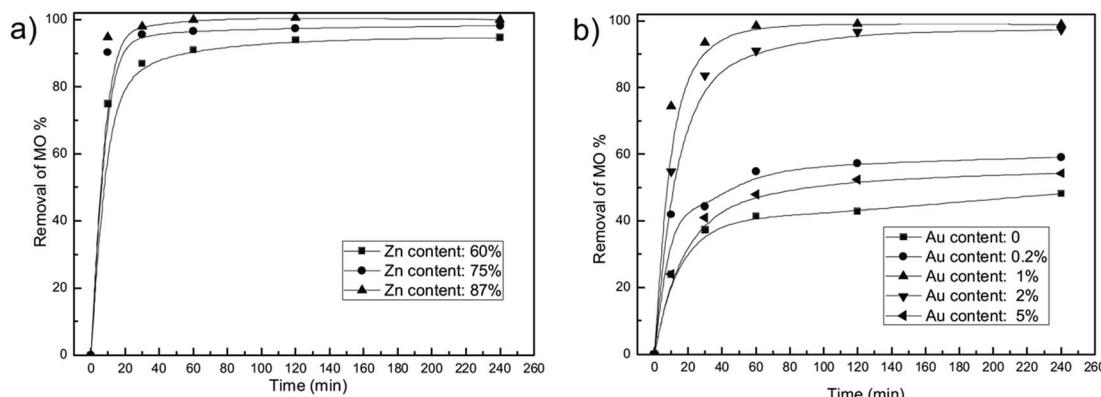
Fig. 7 Effect of material component on MO removal of Au/ZnAl LDO nanocomposites. (a) Different Zn content with constant Au content of 1% and (b) different Au content with constant Zn content of 87% (adapted from ref. 90 with Copyright from 2013 Elsevier).

Mg–Al LDH was prepared *via* a homogeneous precipitation process, the sample exhibited a good sorption capacity of 242 mg g^{-1} for ARG.[110] The same study group synthesized ZnO nanoparticles immobilized on flaky layered double hydroxides as enhanced adsorption for removal of ARG, which resulted in specific surface area of FLDHs (249 m^2 g^{-1}) and a short adsorption equilibrium time.[111]

Using magnetic LDH nanoparticles has aroused great interests for the removal of dyes from aqueous solutions. The magnetic adsorbent with adsorbed dye can be easily separated magnetically and recycled after catalytic regeneration with advanced oxidation technology. Several researchers have investigated the use of magnetic LDH nanocomposites in the removal of dyes molecular. Yang *et al.*[91] synthesized reduced graphene oxide, zero-valent nickel, and Ni–Al mixed metal oxides (rGO/Ni/MMO) by calcining graphene oxide (GO)/layered double hydroxide (LDH) for the purpose of removing MB and found it to be very effective (210.8 mg g^{-1}) compared to GO/MMO at equilibrium 72.6 mg g^{-1}. The high adsorption ability of the hybrid may benefit from the hybrid with less carboxyl groups and small-sized nanoparticles.[112–114] Taking advantage of unique magnetic response and large surface area of magnetic Fe$_3$O$_4$. Chen *et al.*[71] prepared the novel magnetic Fe$_3$O$_4$/Zn–Cr LDH and applied it to remove MO. The material had an excellent adsorption capacity (528 mg g^{-1}), which resulted from the higher surface area (114 m^2 g^{-1}). The same research group subsequently synthesized the same material from electroplating wastewater and studied the adsorption of MO from heavy metal wastewater. The maximum capacity of MO was found to be 240.16 mg g^{-1}, at the same time 99% of heavy metal ions can be effectively removed into precipitates. In addition, this material with adsorbed dye can be easily separated by a magnetic field (Fig. 8).[70]

From the above literature study, it is clear that modified LDHs achieve a higher dye removal ratio as compared to the virgin LDHs. This is because of the larger surface area and functional groups generated by the modification. The surface and functional groups act as active sites which are easily accessible to the dye molecules.

2.3.6. Effect of contact time and initial dye concentration. The contact time between the dyes and the LDH is a vital parameter in the adsorption. In general, adsorption of dyes increases with increasing of contact time and the removal of the adsorbate species is rapid at first and then slows down to near equilibrium. It is because the adequate free adsorptive sites and a high dye concentration gradient during the initial time. Afterwards, the remaining vacant sites are less available for adsorption because of the repulsive forces that occur between the adsorbed and free molecules with time.[59] The relation between removal of MO and contact time were studied to see the rate of dye removal. The high adsorption rate within the initial 1.8×10^3 s was attributed to the adequate free adsorptive sites and a high dye concentration gradient.[10]

The corresponding pore size distributions of the uncalcined and calcined Mg–Ni–Al LDH and the experimental results of MO adsorptions at various initial concentrations with contact time are shown in Fig. 9. The calculated percentage of MO removal decreased from 95% to 86.8% with initial MO concentration increasing from 20 to 100 mg L^{-1}. The calcined LDH performed a better adsorption percent than the uncalcined LDH because the pore volume of the Mg–Ni–Al LDH increased by heating. The difference between equilibrium time obtained with Mg–Ni–Al LDH and calcined Mg–Ni–Al LDH could be explained by the fact that MO anions adsorption onto calcined Mg–Ni–Al occurs by surface and ion exchange phenomena by reconstruction.[58] For a given adsorbent dose the total numbers of available adsorption sites are fixed, thereby the same amount of dyes could be adsorbed. The removal percentage of AC 97 onto Zn$_2$–Al LDH decreased with an increase in initial dye concentration. That resulted from the ratio of initial mole numbers of AC 97 to the available surface area was high at a higher initial concentration.[65]

2.3.7. Effect of competitive anions. The co-existence anions will affect the process of desired contaminates and there are
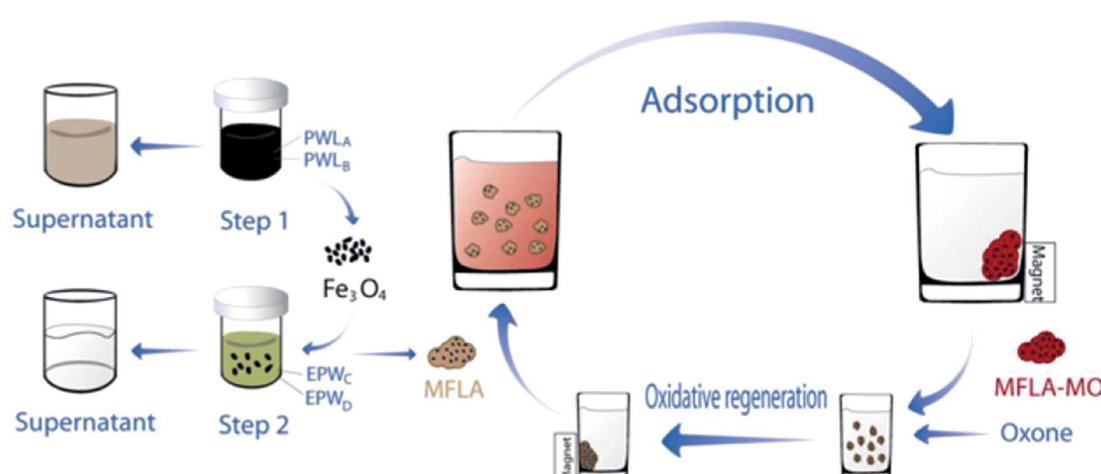
Fig. 8 Synthesis route of MFLA and their application for removal of MO with the help of an external magnetic field (MFLA: magnetic Fe$_3$O$_4$/Zn−Cr LDH adsorbent, PWL: pickling waste liquor, EPW: electroplating wastewater. Adapted from ref. 70 with Copyright from 2012 Elsevier).
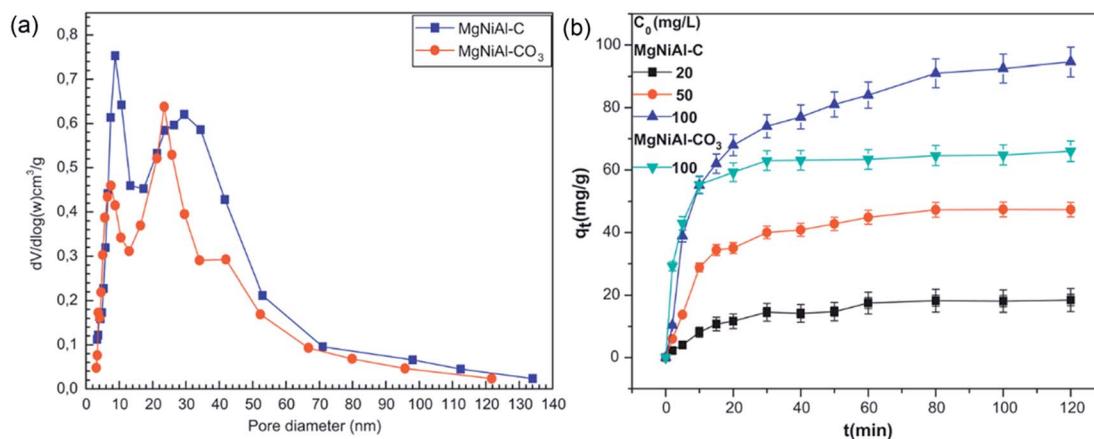
Fig. 9 The pore size distribution curves (a) and effect of time and initial concentration and (b) in the adsorption of MO on the two samples (adapted from ref. 58 with Copyright from 2012 Elsevier).

a few literature reporting the competitive anions on dyes adsorption by LDHs.

The effects of competing anions SO_4^{2-}, Cl^- and CO_3^{2-} on BBR sorption by CLDHs were invested, the effects of SO_4^{2-} and Cl^- on the process were minimal although the molar ratios of Cl^- or SO_4^{2-} to BBR were up to 12. The adsorption even slightly increased with the increment of molar ratios from 2 to 12, which was probably caused by a salting out effect. Evidently, the dyes are not "pushed out" from the sorbent by inorganic salts, which is important feature for potential applications to real wastewaters.[106] Unlike the performance of Cl^- and SO_4^{2-}, the presence of CO_3^{2-} suppressed the sorption, due to the fact that the previously existing interlayer CO_3^{2-} ions in LDHs are difficult to be exchanged by other anions.[34,115] However, for the case of CO_3^{2-}, the CLDH still demonstrated a high sorption capacity for AB 14 even at a high concentration of CO_3^{2-}.[33] In the case of MO adsorption on calcined Zn–Al LDH, the influence of competing anions was reported to follow the order PO_4^{3-} > CO_3^{2-} > SO_4^{2-} > NO_3^- > Cl^-, which confirmed that the divalent anions had more effect on MO adsorption compared to the monovalent anions.[88] In another study of MO adsorption by uncalcined and calcined Mg–Ni–Al LDH. The results showed that adsorption of MO decreased with increasing NaCl concentration. With the increasing ionic strength, the adsorption capacity decreases due to the competing Cl^- anions with MO for surface adsorption.[58]

In general, it could be concluded that the anions of higher valence have a more significant interfering effect than the monovalent anions in the dyes adsorption by calcined LDHs. Among the anions, PO_4^{3-} and CO_3^{2-} appear to be the most competitive anions in the adsorption. Unfortunately, large questions remain as to how competing species regulate the adsorption and existed in the hydroxides, compelling evidence in this regard is currently lacking.

2.4. Mechanism of sorption

Adsorption are defined as the accumulation of a substance or material at an interface between the solid surface and the bathing solution.[116] Mechanism studies of dyes adsorbed by

LDHs have been carried out with either the assistance of the characterization of the structures of the LDHs before and after adsorption such as FTIR, XRD, TEM and SEM, or the postulation from comprehensive experimental observations on sorption kinetic and sorption isotherm. Generally, the dyes may be removed by LDHs *via* (1) surface adsorption (2) interlayer anion exchange (3) reconstruction/memory effect of calcined LDH precursors (4) electrostatic interactions.[53,69,117]

It has been found that many organic compounds have a strong affinity to the surface of clay minerals. The surface adsorption involves the adhesion of dyes to the LDHs surface. Clearly, the parameter of sorbent surface area plays a significant role in this mechanism.[82] The prepared ZnO–LDHs with different mass ratios have different specific areas and the one having a larger surface area shows a stronger adsorption capacity.[110] For the adsorption of AB 9, the powder XRD analysis showed no obvious change in the $d_{(003)}$ spacing. Thus, at low concentration surface adsorption of the dye occurred.[52]

An anion exchange mechanism also plays an important role. The level of exchange depends on the substituent anions, M^{2+}/M^{3+} ratio and the anions to be intercalated.[53,97] Some ligands were intercalated to form organic–inorganic composite adsorbents, the intercalated sodium alginate helps in widening the interlayer space of the hydrotalcite-like anionic clays, making them accessible for intercalation of orange II dye.[118] The adsorption of MO and GR onto Ca–Al LDH was studied by X-ray diffraction (XRD), infrared spectroscopy (MIR), scanning electron microscope (SEM), and near-infrared spectroscopy (NIR). All results indicated that MO ion was intercalated into Ca–Al LDH interlayers, and acidic scarlet GR was only adsorbed upon Ca–Al LDH surfaces.[119] The mechanism of these interaction models is displayed in Fig. 10. Anion exchange may also happen on the surface. The surface carbonates or hydrogen carbonates are easily replaced by anionic dyes, and anion exchange can still be achieved even if the original interlayer anion is carbonate an ion that can be difficult to exchange from the LDH interlayer region.[52] In the adsorption of AB 14 dye on Mg–Fe LDH, the result showed that the interlayer distance changed a little, meaning the exchange occurred mainly on the outer planner
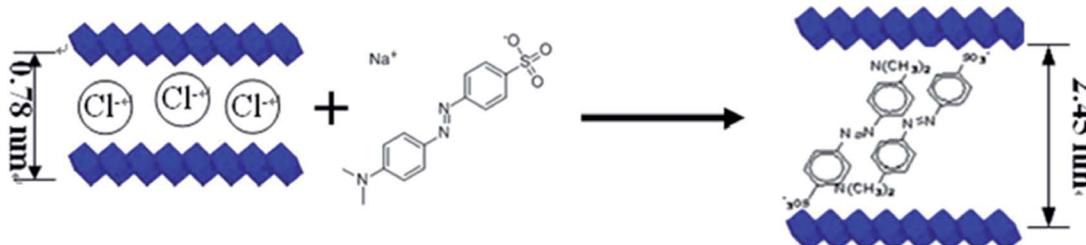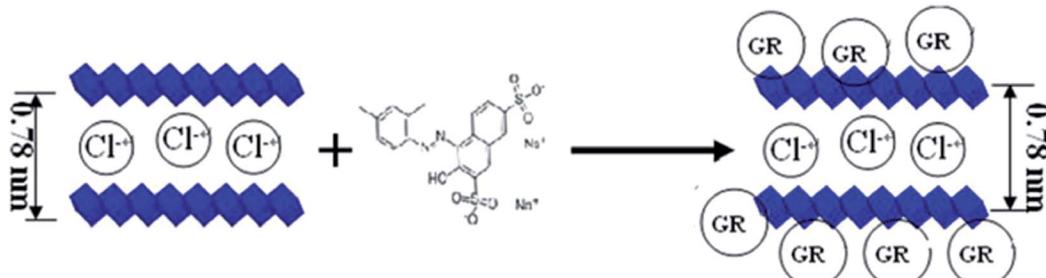
Fig. 10 The models illustration of MO and GR interacted with Ca–Al LDH (adapted from ref. 119 with copyright from 2012 Elsevier).

surfaces and at the edges of inter-layers in LDH containing CO_3^{2-}.[33]

Electrostatic interactions happened between the groups of the dye and the ligands intercalated into interlayers and this usually used for the removal of cationic dyes. Researchers synthesised heteropoly blue intercalated layered double hydroxide. The intercalation of large cluster anion $[PW_{10}Mo_2O_{40}]^{5-}$ into LDH could induce the adsorption of cationic dye of MB onto HB–LDH, obviously. The HB–LDH shows much higher cationic dye adsorption capacity than pure LDH and the maximum adsorption capacity of MB was 30.87 mg g^{-1}.[69] Wei et al.[74] prepared DGLN–LDHs hybrid to adsorb victorial blue B, through the electrostatic interactions between the DGLN and LDHs (Fig. 11), which was confirmed by the FTIR, resulting in the adsorption capacity of 1064 mg g^{-1}.

Majority of studies related to the removal dyes by calcined LDH revealed predominant adsorption mechanism is reconstruct of the original layered structure in an aquatic environment, as expressed as follows:[33]

$$[Mg_{1-x}Fe_x(OH)_2](CO_3)_{x/2} \rightarrow Mg_{1-x}Fe_xO_{1+x/2} + (x/2)CO_2 + H_2O \quad (1)$$

$$Mg_{1-x}Fe_xO_{1+x/2} + (x/n)A^{n-} + (x)AB\ 14 + (1 + x/2)H_2O \rightarrow Mg_{1-x}Fe_x(OH)_2(AB\ 14)_x + xOH^- \quad (2)$$
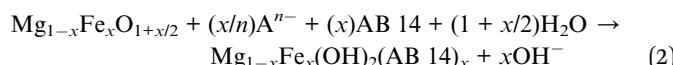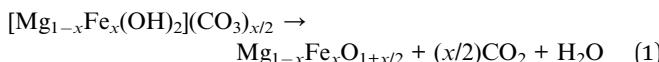
The adsorption mechanism is presumed that the CLDH reconstructed the layered structure after adsorption of AB 14, the anions of AB 14 intercalated into the interlayer of LDH by chemisorptions. Ni et al.[88] studied the treatment of MO by calcined Zn–Al LDH and presumed a similar adsorption mechanism. Zn–Al LDO reconstructed the layered structure after MO adsorption, the most of interlayer anions are OH^-, however, there are parts of MO ions and CO_3^{2-} intercalated into the interlayer of LDH by chemisorption (Fig. 12). Also in the reconstruction process, OH^- ions are simultaneously released. Consequently, final pH of the aquatic solution will be enhanced. This is environmentally meaningful for precipitation or co-precipitation of some co-existing metal cations like Ca^{2+}, Pb^{2+} and Cd^{2+}.[120,121] The reconstruction also makes contribution to a much larger sorption capacity of CLDH than that of LDH resulting from higher surface area and the presence of stronger basic sites. The specific surface area of the Mg–Ni–Al LDH increased from 137.4 to 246.5 m^2 and the pore volume from 0.451 to 0.590 cm by heating at 500 °C.[58] Another advantage is the shorter equilibrium time. For the sorption of BBR, both film diffusion and pore diffusion were involved in ion exchanges in LDHs, however, structural reconstruction and BBR intercalation occurred almost simultaneously in CLDHs and the processes were obviously rapid.[34] The reconstruction mechanism could also been affected by the exposure time. A surface adsorption mechanism is proposed to account for the adsorption of the dye onto the calcined Mg–Al layered double hydroxides. X-ray powder diffraction analysis indicated that given sufficient time it was possible to intercalate the dye within the layered double hydroxides' interlayer via a reconstruction mechanism.[80]

2.5. The disposal of LDH-dye sludge

After adsorption, how to deal with the adsorbent sludge is of great interest to both scientific research and practical application. There are two main solutions on the disposal of the
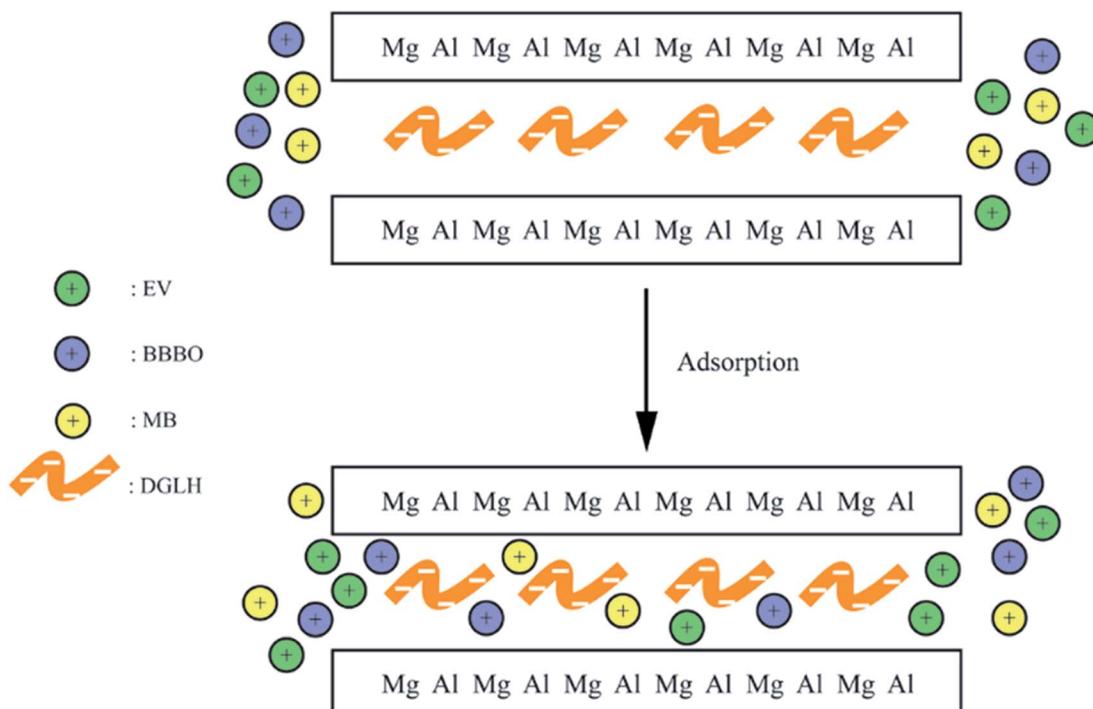
Fig. 11 The proposed adsorption mechanism for cationic dyes with DGLH–LDH.
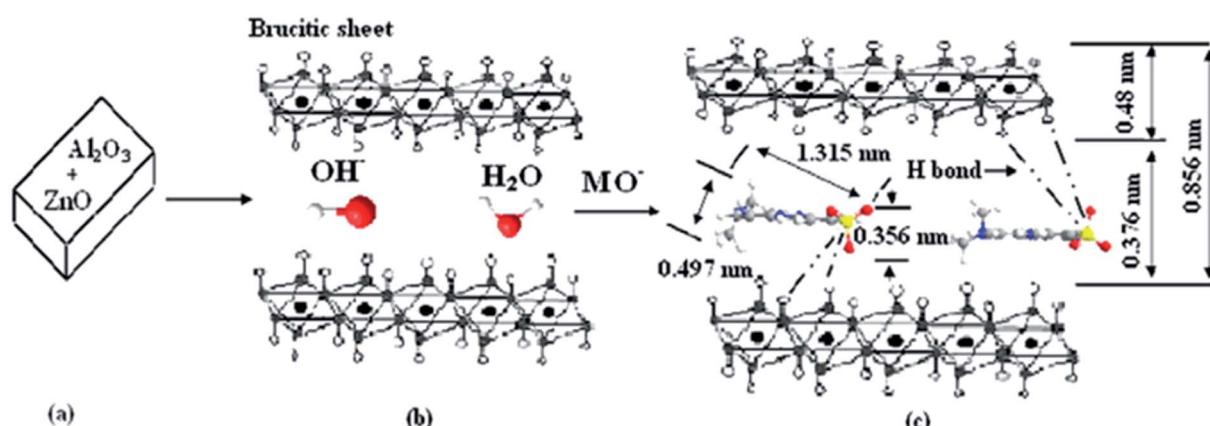
Fig. 12 The schematic illustration of MO adsorption by Zn–Al LDO. (a) The calcined layered double hydroxides. (b) The layered structure of recovered products is restructured by adsorption. (c) MO intercalated into LDH layered by chemisorption (adapted from ref. 88 with copyright from 2007 Elsevier).

resulting sludge: regeneration and reutilization, among which the regeneration is the most frequently used.

Ulibarri et al.[122] proposed that by combustion at 450–500 °C, adsorbed organic pollutants can be almost completely eliminated and LDH or CLDH sorbents can be regenerated into CLDH-like materials based on the "memory effect". A lot of the regeneration tests were carried out by calcining the exhausted adsorbents. However, most of the adsorbent was feasible only within the first three cycles after thermal regeneration.[79,88,95,111] In the removal of BBR, thermal regeneration of LDHs and CLDHs after sorption were feasible only within the first two cycles, after which the regenerated materials suffered from

a large loss in their sorption capacities. The large loss resulted from progressively decreasing crystallinity of the LDHs in structural reconstruction after thermal regeneration, as well as by the incorporation of organic species remnant of the thermally decomposed dye. A similar conclusion was confirmed in the removal of AG 68:1 from aqueous solutions by calcined and uncalcined layered double hydroxides.[53]

A few LDH regeneration studies have been performed by sulfate radical-based oxidation technology[70,91] and acetone extraction.[69,76] Chen et al.[70] recycled the adsorbent after catalytic regeneration with advanced oxidation technology and reported that the adsorption properties of were drastic reduced, due to

the reduction of specific surface area. Bi et al.[69] showed that after the first regeneration cycles by acetone extraction, the removal efficiency of MO decreased from 75% to 33%, which may resulted from an incomplete acetone extraction of the adsorbed dye.

As for the reutilization of the LDH adsorbent sludge, Xue et al.[65] added the LDH adsorbent sludge into polypropylene (PP) and found that the Zn_2Al–AC97 LDH could significantly improve the thermal stability and UV shielding ability of PP. In addition, the resulting sludge was reutilized as a colorant filled in polymer materials and it exhibited the resistance to bleeding and fire.[74]

3. The photocatalytic degradation of dyes by LDH materials

Photocatalytic degradation offers an attractive solution to organic contaminants by completely converting molecular to carbon dioxide, water, and mineral acids.[24,110] A number of

photocatalysts have shown high photocatalytic activity. However, taking into account the large band gap and economic cost, they are unsuitable for treating large amounts of wastewater. Incorporation of photocatalysts in LDHs is a promising strategy for wastewater treatment. The pollutants would not only be adsorbed by LDHs but also degraded, and this could greatly increase the wastewater treatment capacity.

Seen from Table 3, in the context of degradation of dyes, three types of LDHs-based photocatalysts have been hitherto created: (1) direct photocatalysts (2) mixed metal oxide (MMO) materials derived from LDH single precursors (3) supports to photocatalytic guests.

3.1. Direct photocatalysts

LDH was very much promising material for pollutant degradation in advanced oxidative process.[129] With the properties that LDHs have two or three different metals and the ratio among these metals could be varied, LDHs can be regard as "doped semiconductor". Doping or composition would result in a state

Table 3 Summary of LDH-based materials photocatalytic degradation studies of dyes

LDHs	Kinetics of degradation	Dyes	Light irradiation	Ref.
Mg–Al LDH	—	Methylene blue, methyl orange	Vis	123
Ni–Ti LDH	1st	Methylene blue	Vis	124
Cu–Co–Cr LDH	—	Malachite green	Vis	125
Zn–Al LDH	1st	Acridine orange	UV	126
Zn–Al LDH Mg–Al LDH	1st	Methyl orange, fast green	UV	67
Zn/M LDH (M = Al, Fe, Ti, Fe/Ti)	1st	Rhodamine B	Vis	127
Zn_3–Al LDH	—	Methyl orange	UV	51
Zn–Ti LDH	—	Methylene blue	Vis	128
Zn–Cr LDH	—	Methylene blue, methyl orange	Vis	123
Zn–Cr LDH	1st	Rhodamine B, rhodamine 6G	Vis	129
Zn–Fe LDH	—	Methyl violet, malachite green	Vis	130
Zn–Cd–Al LDH	—	Methylene blue	Vis	131
Pt–Zn–Ti LDH	1st	Rhodamine B	Sunlight	11
C–Ni–Mg–Fe–Al LDH	—	Drimaren red, drimaren navy	UV	132
C–Ni–Ti LDH	1st	Methylene blue	UV-Vis	133
C–Zn–Al LDH	—	Methyl orange	UV	134
C–Zn–Al LDH	1st	Methylene blue, methyl orange	UV	135
C–Mg–Zn–In LDH	—	Methylene blue	Vis	136
CeO_2/Zn–Ti LDH	—	Methyl orange, methylene blue	UV	28
C–Bi–Zn–Ti LDH	1st	Indigo carmine	Vis	137
C–CNT/Co–Ni–Al–Zn LDH	—	C.I. acid red 14	Vis	138
C-Legume/Zn–Al LDH	—	Polybenzenesulfonamido sulforhodamine B	UV	139
C–Zn–Al–Ti LDH	1st	Methylene blue, rhodamine B	Vis	140
C–CG–Zn–Al LDH	—	Methylene blue, orange G	Vis	141
C–Ni–Zn–Al LDH	1st	Orange G	Solar	142
TiO_2/Mg–Al LDH	—	Methyl orange	UV	143
TiO_2/Mg_2–Al LDH	1st	Acid orange 7	UV	144
Cu_2O/Mg–Al LDH	—	Methylene blue	Vis	145
ZnO/Mg–Al LDH	—	Acid red G	UV	146
Pd(II)–Bi_2O_3/Mg–Al LDH	1st	Methylene blue	Vis	147
SnO_2/Mg–Al LDH	—	Methylene blue	UV	148
Ag/AgBr/Co–Ni LDH	—	Methyl orange	UV/Vis	149
BiOBr/Co–Ni LDH	—	Methyl orange, rhodamine B	UV	150
TiO_2/Cu–Mg–Al RLDH	—	Methylene blue	UV/Vis	151
Fe_3O_4/Zn–Cr LDH	1st	Methylene blue, methyl orange	UV	71
CuPcTs/Zn–Al LDH	—	Methylene blue	Solar	152
MoO_4^{2-}/WO_4^{2-}–Zn–Y LDH	1st	Rhodamine 6G	Vis	153
M_xO_y/Zn–Ti LDH (M = Fe, Sn, Ce)	1st	Acid red 14	Vis	154

of defect energy between the valence band and conduction band, which would provide a spring board for photon generated electrons (e^-). And this photon generated electrons can activate valence band electrons transmit to conduction band by visible light with lower energy, which would make the absorption edge move to visible light region. Thus, it would reduce the band gap energy of materials, and also improve the photo-catalytic property.[28] Some works aimed at revealing the role of pristine layered double hydroxide (LDH) materials in the elimination of organic pollutants from solution.

M^{2+}–Ti LDHs were synthesized and confirmed that the doping of Ti into LDHs could improve the catalytic ability of dyes.[28,127,128] Zn–Ti LDH was synthesized and resulted in high visible light photocatalytic activity for MB, which resulted from the lower band gap, the hierarchical structure and high specific surface. The high specific surface area would provide strong adsorption ability toward target dyes and lead to the generation of photoinduced electron–hole pairs of active sites. A wide distribution of macropores is favorable for the transportation and diffusion of species.[128,155,156] Xia et al.[28] observed the photocatalytic degradation performance of MO and MB by three Ti-based layered double hydroxides, which followed the order: CeO₂/Zn–Ti LDHs > Zn/Al–Ti/SB LDHs > Zn/Ti LDHs. The same group also checked the degradation performance of RB by a series of Zn/M–LDHs (M = Al, Fe, Ti, and Fe/Ti) and found that after three regeneration cycles, the percentage degradation rate was still close to 90%.[127] These phenomenon were attributed to the basis of electronic structure property and textural parameters of LDH. Some other researchers also reported that surface areas, pore volume pore size distribution and crystallite size lead to the promotion of photo-induced degradations of dyes.[67,128,130,134]

Silva et al.[157] developed a novel series of visible active Zn–M (M = Cr, Ti, Ce) LDH photocatalysts for oxygen generation from water and the result showed that it can be regarded as a "doped semiconductor" in which 'M (III)' used as dopant. These findings motivates researcher to further study the semiconductor properties of Zn–M LDH materials in the degradation of dyes. Zn–Cr LDH were prepared and used for the removal of MB, MO[123] and xanthene dyes,[129] the study demonstrated that Zn–Cr LDH was an efficient photocatalyst for degradation of organic pollutants, but the rapid charge recombination and low efficiency in electron/hole separation would suggest that photocatalytic activity would be greatly limited.[123] A novel magnetic Fe₃O₄/Zn–Cr LDH composite was successfully fabricated and the results revealed a higher removal of dye on the composite, compared to that on Zn–Cr LDH under the same conditions.[71] K. M. Parida[130] synthesized Zn–Fe LDH with different intercalated anions and studied the photodegradation of MV and MG under solar light, the tentative mechanism may be photocatalytic degradation (mineralization):[130]

$$\text{Catalyst} + h\nu \rightarrow \text{Catalyst} (e_{CB}^- + h_{VB}^+) \qquad (3)$$

$$\text{Catalyst} (h_{VB}^+) + H_2O \rightarrow \text{Catalyst} + H^+ + OH^\cdot \qquad (4)$$

$$\text{Dye} + OH^\cdot \rightarrow \text{Dye product (DP)} \qquad (5)$$

$$\text{Catalyst} (e_{CB}^-) + O_2 \rightarrow \text{Catalyst} + O_2^{-\cdot} \qquad (6)$$

$$O_2^{-\cdot} + \text{Dye} \rightarrow \text{Dye product (DP)} \qquad (7)$$
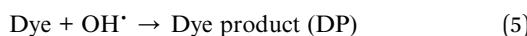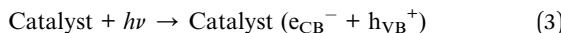
3.2. Mixed metal oxide (MMO) materials

After being calcined under high temperature, bimetallic oxide could be formed, the second metal could be high dispersed and doped into the LDH materials, and then the photocatalysis of these materials could be dramatically improved. In particular, the mixed oxides derived from Zn, Al containing LDHs without or with Fe, Sn and Ti, are successful photocatalysts for the degradation of organic compounds like MO, MB and phenols in aqueous media.[140]

The Zn–Al LDH samples were calcined at different temperatures and found that the band gap energy decreased as the calcination temperature increased. The photocatalytic activity is highly improved when samples are calcined at 500 °C due to the large amounts of ZnO phase formed.[134] In another study, ZnO/ZnAl₂O₄ composite photocatalyst was prepared by calcining Zn–Al LDH and also showed a high degradation efficiency of MB and MO. The calcined Ni–Ti LDH nanocomposite particles were photoresponsive in the UV-VI region and indeed exhibited good photocatalytic activity for MB.[133] Zhao et al.[139] reported the fabrication of biotemplated LDH film and MMO framework from the legume and demonstrated its effective and recyclable photocatalysis (recyclable for even 6 times) for the decomposition of two kinds of dyes due to its large specific surface area and wide pore size distribution.

LDHs containing tetravalent cations have been synthesized to explore the possibility for photocatalytic degradation of various dyes.[125,132,136,140] The degradation performance of MB and RhB was found to increase slowly with the increase of Ti content in the calcined Zn–Al–Ti LDH catalyst. This increased activity may be attributed to resultant effects of decreased band gap energy and BET surface area.[140] By the isomorphous replacement of Zn for Mg in coprecipitation system and the photocatalytic performance of Mg–Zn–In ternary layered materials have been invested by Li Huang.[136] The research group found that the presence of Mg in the composite could improve the stability of the catalyst and doping zinc into the Mg–In system enlarged the surface area as well as the pore volume of calcined sample. The ternary Mg–Zn–In layered photocatalyst exhibits a considerably high activity in the degradation of MB resulted from the special structure of LDH. Both of the studies involved dye-sensitized process and the overall photocatalytic process schematically presented in Fig. 13.

Enrichment of reactants by adsorption is required for a highly efficient photocatalytic performance.[158,159] After calcination, the large surface areas of the MMO produce a large amount of electron/hole pairs and ensure the adsorption of dye molecule to the active sites, therefore the catalytic efficiency is enhanced.[160] The high dispersion of MMO nanocrystals and wide pore size distribution not only benefit the transfer of the light-generated charge carriers to the surface to react with dye
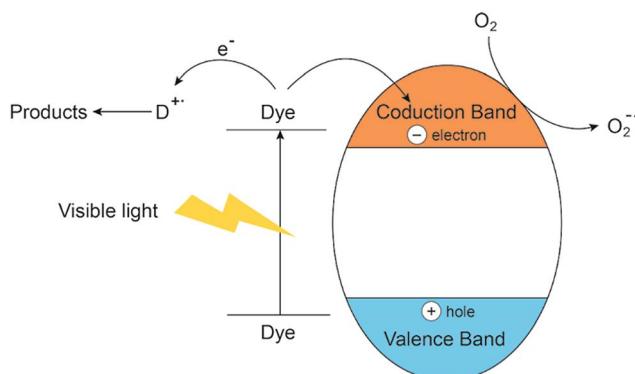
Fig. 13 Electron transfer process from the excitation of dye in the visible region.

molecules but also allow fast diffusion of reactants and products. In addition, the samples would be a relatively lower band gap energy after calcination. All these factors make the calcined LDHs showing better activities than the uncalcined LDHs.

3.3. Supports to photocatalytic guests

Semiconducting photocatalysts have attracted extensive attention due to their potential industrial applications.[161] Semiconductor photocatalysts generates electrons and hole pairs (e^-/h^+) upon irradiation with light energy that can be utilized in initiating oxidation and reduction reactions, respectively. Nevertheless, the recombination of holes and electrons or agglomeration of the fine nanoparticles may lead to a decreased photocatalytic activity. Therefore, it is especially interesting to support semiconductor on suitable substrates for wastewater remediation.[143] One of the attractive materials utilized to enhance photocatalytic activities of semiconductors-based materials is layered double hydroxides.[135]

It was previously reported that the materials rich in OH groups, like LDHs, may favor the titania activity. The surface hydroxyl groups may be easily converted into HO$^{\bullet}$ radicals, which are the primary species responsible for the dye degradation.[162,163] Lu *et al.*[151] fabricated supported TiO_2 nanoparticles and proved TiO_2/Cu–Mg–Al LDH sample has superior photocatalytic properties to the rehydrated single phase R-TiO_2. The TiO_2/LDH heterojunction nanostructure is proposed to contribute to the efficient spatial separation between the photogenerated electrons and holes, which can concomitantly improve the photocatalytic activity. The influence of initial Ti^{4+} location on the quality of the LDHs-type materials was studied and the $Mg_3Al_{0.5}Ti_{0.5}$–LDH sample showed powerful photooxidative effect assigned to the segregation of small anatase nanocrystals on the highly hydroxylated layered surface.[143] A new materials colloidal TiO_2/LDH was prepared for photodegradation of AO7, a high surface area and the great adsorption of TiO_2/LDHs particles facilitated electron injection so that a significant increase of the photodegradation rate of AO7 was obtained.[144]

Apart from TiO_2/LDH composites, other hybrid photocatalysts have been researched for the decomposition of dyes

such as NanoPt–LDH,[11] CuPcTs–LDH,[152] ZnO–FLDH, SnO_2–LDH,[148] Ag/AgBr/Co–LDH,[149] $MoO_4{}^{2-}/WO_4{}^{2-}$–LDH.[130] A new SnO_2/Mg–Al LDH was obtained for MB degradation. The proposed mechanism was based on the shifting of flat band potential of SnO_2 due to the interaction with Mg–Al LDH, this being energetically favourable to the formation of hydroxyl radicals responsible for methylene blue degradation.[148] Another Ag/AgBr/Co–LDH nanomaterials have been developed as photocatalysts, the photoinduced holes in the VB of AgBr could easily induce formation of $^{\bullet\bullet}$OH from OH groups of the LDH and these oxidative species would result in degradation of dyes, as shown in Fig. 14.[149]

Above all, incorporation of photocatalysts into LDHs is a promising strategy for dye degradation. The pollutants would not only be adsorbed on the surface of LDHs, but also be degraded, and this can greatly increase the wastewater treatment capacity.

3.4. Kinetics of degradation

The kinetics of degradation dyes catalyzed by LDH materials were investigated based on the Langmuir–Hinshelwood model, which was widely used to describe the kinetics of photocatalytic reactions of dyes compounds in aqueous solutions.[164] When the concentration of organic compounds is low and the adsorption is relatively weak, the equation can be simplified as follows:

$$r = K_r K_{ad} C = K_{app} C \qquad (8)$$

Setting eqn (1) under initial conditions of photocatalytic procedure, ($t = 0$, $C = C_0$), eqn (2) is obtained:

$$\ln \frac{C_0}{C} = K_{app} \qquad (9)$$

where C_0 and C are the initial concentration of dye and the concentration at time t, respectively. The values of apparent rate constant (K_{app}) can be calculated from the gradient of the graph of $\ln(C_0/C)$ *vs.* irradiation time by regression method.[28] Further, the plots of $\ln(C/C_0)$ *versus* irradiation time are straight lines indicating that the degradation of dyes follows a first order kinetics.[140] As shown in Table 3, the photodegradation process generally obeys pseudo-first-order kinetics. Xia *et al.*[28] demonstrated CeO_2/Zn–Ti LDH composite was considerably effective for MO and MB through the photodegradation lineal plot and
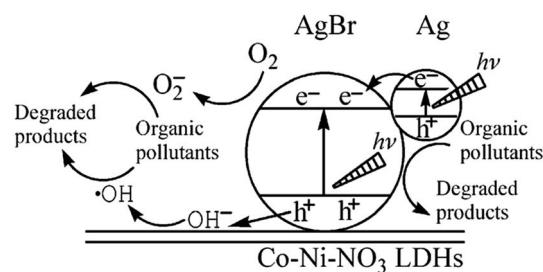
Fig. 14 Schematic photocatalytic mechanism of Ag/AgBr/Co–Ni–NO_3 LDH nanocomposites under visible-light illumination (adapted from ref. 149 with Copyright from 2013 Wiley).

the rate constant. In the photocatalytic degradation of RhG, the apparent reaction rate constants (k_{app}) and the $t_{1/2}$ parameters were evaluated from experimental data using a linear regression, the result confirmed that k_{app} was enhanced in the molybdate intercalated LDH.[153]

4. Conclusion and future perspectives

In summary, LDHs has been applied to construct different and promising sorbents and catalysts. By incorporated with nanoparticles or other substances, LDHs can offer their unique properties and possibly induce new performance. The use of LDHs in the removal of dyes results in markedly improved adsorption capacity and photocatalytic degradation efficiency over other conventional materials. A survey of the literature on the synthesis of LDHs reveals calcination, nanomaterials, inorganic oxides and surfactant have been used to enhance the adsorption performance. An analysis of adsorption mechanisms reveals that the surface adsorption, anion exchange and reconstruction are predominantly responsible for binding the organic pollutants. The main advantages of LDHs over the conventional anionic exchange resins include their higher anion exchange capacity for certain anion and their good thermal stability. LDHs and LDHs based materials (mixed metal oxide materials and supports to photocatalytic guest) are applied to degrade dyes and received a higher degradation percent as the result of extended light adsorption range and excellent charge separation–transportation capability.

Although considerable progresses have been achieved in the field of adsorption and degradation of dyes by LDHs, the studies in wastewater remediation need to be further developed, at least, the following aspects should be considered:

(1) Most of the adsorption studies focused on the anionic dyes, only a few cases were on the removal of cationic dyes. Multi-purpose, economically feasible composites should be developed to remove not only for the anionic dyes but also for the cationic and nonionic dyes.

(2) An understanding of the adsorption process and photocatalytic degradation in the multi-dyes system should be totally understood. The mechanisms in both of the adsorption and photocatalytic degradation process should be explained by a variety of analytical tools.

(3) It is important to estimate the cost of any adsorption system or degradation system. However, LDHs have not been used at a commercial level to any extent, there is no data available to estimate the cost of production and application. An evaluation of the cost of LDHs between other low-cost sorbent should be encouraged and develop an economical and environment-friendly way to make use of the LDH-dye sludge.

(4) Finding the most appropriate element ratio, optimum surface area and calcination temperature to synthesize the LDHs for the particular dye to obtain a better removal percent. Since the release of the binding inorganic and organic glands would cause secondly pollution, using the environment-friendly modificators in the synthetic system is necessary.

(5) Attempts have been made to intercalate various dye molecules, in particular organic dyes inside layered inorganic lamella. Mg–Al LDH intercalated with Coomassie Brilliant Blue R anion was prepared to take up aromatic compounds from aqueous solutions.[165] Evan's Blue incorporation into the Mg–Al LDH to form an organic–inorganic nanohybrid composite material was reported. Formation of such a material is useful, for example for controlled release purposes of dye for slow dyeing process.[166] These developments of new organic–inorganic hybrid type materials open promising prospects for the reutilization of the LDH-dye sludge after adsorption.

(6) The development of new approach for preparation of novel based LDHs photocatalytic materials with improved activity and stability working in visible-light region is still highly valued. It is highly desirable to develop efficient visible-light driven photocatalysts that predominantly take advantage of solar energy and indoor illumination in the visible-to-infrared range.

(7) Designing and fabrication of an economically cheap treatment for the removal of dyes from diluted industrial effluent and invent a treatment system *via* combing the LDH adsorption with photocatalysis technology to improve the performance.

5. Abbreviations

AB 9	Acid blue 9
AB 14	Acid brown 14
AB 113	Acid blue 113
AB 29	Acid blue 29
ARG	Acid red GR
AR 1	Acid red 1
AO 7	Acid orange 7
AG 68:1	Acid green 68:1
AY 23	Acid yellow 23
AR 37	Acid red 37
BBR	Brilliant blue R
CG	Carboxyl graphene
CLDH	Calcined LDH
CNT	Carbon nanotubes
CR	Congo red
DA	Dodecanoic acid
DGLN	Direct blending scarlet D-GLN
F	Freundlich
GB-F2B	Green bezanyl-F2B
GO	Graphene oxide
GR	Acidic scarlet GR
HB	Heteropoly blue
ILs	Hydroxyl ammonium ionic liquids
I-P	Intra-particle diffusion
L	Langmuir
LDO	Layered double oxides
MB	Methylene blue
MG	Malachite green
MMH	Mixed metal hydroxide
MO	Methyl orange
MV	Methyl violet

OG	Orange G
OII	Orange II
RBR K-2BP	Reactive brilliant red K-2BP
RhB	Rhodamine B
RhG	Rhodamine 6G
R–P	Redlich–Peterson
RR 3BS	Remazol red 3BS
RY	Reactive yellow 4 GL
SDS	Sodium dodecylsulfate
1st	Pseudo-first-order
2nd	Pseudo-second-order

Acknowledgements

References

1 G. Zeng, M. Chen and Z. Zeng, *Science*, 2013, **340**, 1403.

2 S. Li, *Bioresour. Technol.*, 2010, **101**, 2197–2202.

3 N. Bao, Y. Li, Z. Wei, G. Yin and J. Niu, *J. Phys. Chem. C*, 2011, **115**, 5708–5719.

4 J. Zhang, S. Chen, Y. Zhang, X. Quan, H. Zhao and Y. Zhang, *J. Hazard. Mater.*, 2014, **274**, 198–204.

5 M. Kornaros and G. Lyberatos, *J. Hazard. Mater.*, 2006, **136**, 95–102.

6 J. Labanda, J. Sabaté and J. Llorens, *Chem. Eng. J.*, 2011, **166**, 536–543.

7 Y. Zheng, G. Yao, Q. Cheng, S. Yu, M. Liu and C. Gao, *Desalination*, 2013, **328**, 42–50.

8 J. L. Gong, B. Wang, G. M. Zeng, C. P. Yang, C. G. Niu, Q. Y. Niu, W. J. Zhou and Y. Liang, *J. Hazard. Mater.*, 2009, **164**, 1517–1522.

9 D. Rajamanickam and M. Shanthi, *Spectrochim. Acta, Part A*, 2014, **128**, 100–108.

10 L. Ai, C. Zhang and L. Meng, *J. Chem. Eng. Data*, 2011, **56**, 4217–4225.

11 Q. Fang and B. Chen, *J. Mater. Chem. A*, 2014, **2**, 8941.

12 S. Dong, J. Feng, Y. Li, L. Hu, M. Liu, Y. Wang, Y. Pi, J. Sun and J. Sun, *Appl. Catal., B*, 2014, **152–153**, 413–424.

13 S. Dong, J. Sun, Y. Li, C. Yu, Y. Li and J. Sun, *Appl. Catal., B*, 2014, **144**, 386–393.

14 S. Dong, Y. Cui, Y. Wang, Y. Li, L. Hu, J. Sun and J. Sun, *Chem. Eng. J.*, 2014, **249**, 102–110.

15 S. Dong, J. Feng, M. Fan, Y. Pi, L. Hu, X. Han, M. Liu, J. Sun and J. Sun, *RSC Adv.*, 2015, **5**, 14610–14630.

16 V. K. Gupta, R. Kumar, A. Nayak, T. A. Saleh and M. A. Barakat, *Adv. Colloid Interface Sci.*, 2013, **193–194**, 24–34.

17 M. Hua, S. Zhang, B. Pan, W. Zhang, L. Lv and Q. Zhang, *J. Hazard. Mater.*, 2012, **211–212**, 317–331.

18 L. Yu and Y.-m. Luo, *J. Environ. Chem. Ecotoxicol.*, 2014, **2**, 220–229.

19 M. Toor and B. Jin, *Chem. Eng. J.*, 2012, **187**, 79–88.

20 P. Xu, G. M. Zeng, D. L. Huang, C. L. Feng, S. Hu, M. H. Zhao, C. Lai, Z. Wei, C. Huang, G. X. Xie and Z. F. Liu, *Sci. Total Environ.*, 2012, **424**, 1–10.

21 D. Sun, X. Zhang, Y. Wu and X. Liu, *J. Hazard. Mater.*, 2010, **181**, 335–342.

22 C. A. P. Almeida, A. dos Santos, S. Jaerger, N. A. Debacher and N. P. Hankins, *Desalination*, 2010, **264**, 181–187.

23 G. Crini, *Bioresour. Technol.*, 2006, **97**, 1061–1085.

24 V. K. Gupta, R. Jain, A. Mittal, M. Mathur and S. Sikarwar, *J. Colloid Interface Sci.*, 2007, **309**, 464–469.

25 K. M. Lee, C. W. Lai, K. S. Ngai and J. C. Juan, *Water Res.*, 2016, **88**, 428–448.

26 L. Ćurković, D. Ljubas, S. Šegota and I. Bačić, *J. Alloys Compd.*, 2014, **604**, 309–316.

27 P. Muthirulan, C. N. Devi and M. M. Sundaram, *Ceram. Int.*, 2014, **40**, 5945–5957.

28 S. J. Xia, F. X. Liu, Z. M. Ni, W. Shi, J. L. Xue and P. P. Qian, *Appl. Catal., B*, 2014, **144**, 570–579.

29 J. Wang, Y. Wei and J. Yu, *Appl. Clay Sci.*, 2013, **72**, 37–43.

30 F. Kovanda, E. Jindová, K. Lang, P. Kubát and Z. Sedláková, *Appl. Clay Sci.*, 2010, **48**, 260–270.

31 X. Liang, Y. Zang, Y. Xu, X. Tan, W. Hou, L. Wang and Y. Sun, *Colloids Surf., A*, 2013, **433**, 122–131.

32 L. El Gaini, M. Lakraimi, E. Sebbar, A. Meghea and M. Bakasse, *J. Hazard. Mater.*, 2009, **161**, 627–632.

33 Y. Guo, Z. Zhu, Y. Qiu and J. Zhao, *Chem. Eng. J.*, 2013, **219**, 69–77.

34 M. X. Zhu, Y. P. Li, M. Xie and H. Z. Xin, *J. Hazard. Mater.*, 2005, **120**, 163–171.

35 L. Shao, Y. Yao, S. Quan, H. Wei, R. Wang and Z. Guo, *Mater. Lett.*, 2014, **114**, 111–114.

36 H. A. Z. E. Ghorbani and Z. Talleb, *J. Iran. Chem. Soc.*, 2013, 1103–1112, DOI: 10.1007/s13738-013-0255-z.

37 C. Forano, T. Hibino, F. Leroux and C. Taviot-Guého, in *Developments in Clay Science*, ed. B. K. G. T. Faïza Bergaya and L. Gerhard, Elsevier, 2006, vol. 1, pp. 1021–1095.

38 Y. Zhong, Q. Yang, K. Luo, X. Wu, X. Li, Y. Liu, W. Tang, G. Zeng and B. Peng, *J. Hazard. Mater.*, 2013, **250–251**, 345–353.

39 C. G. Silva, Y. Bouizi, V. Fornés and H. García, *J. Am. Chem. Soc.*, 2009, **131**, 13833–13839.

40 M. T. Yagub, T. K. Sen, S. Afroze and H. M. Ang, *Adv. Colloid Interface Sci.*, 2014, **209**, 172–184.

41 W. S. Wan Ngah, L. C. Teong and M. A. K. M. Hanafiah, *Carbohydr. Polym.*, 2011, **83**, 1446–1456.

42 K. H. Goh, T. T. Lim and Z. Dong, *Water Res.*, 2008, **42**, 1343–1368.

43 Z. P. Xu, J. Zhang, M. O. Adebajo, H. Zhang and C. Zhou, *Appl. Clay Sci.*, 2011, **53**, 139–150.

44 M. J. Barnabas, S. Parambadath, A. Mathew, S. S. Park, A. Vinu and C. S. Ha, *J. Solid State Chem.*, 2016, **233**, 133–142.

45 R. Lafi, K. Charradi, M. A. Djebbi, A. Ben Haj Amara and A. Hafiane, *Adv. Powder Technol.*, 2016, **27**, 232–237.

46 R. r. Shan, L. g. Yan, Y. m. Yang, K. Yang, S. j. Yu, H. q. Yu, B. c. Zhu and B. Du, *J. Ind. Eng. Chem.*, 2015, **21**, 561–568.

47 G. Darmograi, B. Prelot, G. Layrac, D. Tichit, G. Martin-Gassin, F. Salles and J. Zajac, *J. Phys. Chem. C*, 2015, **119**, 23388–23397.

48 M. Zhang, Q. Yao, C. Lu, Z. Li and W. Wang, *ACS Appl. Mater. Interfaces*, 2014, **6**, 20225–20233.

49 Y. Li, B. Gao, T. Wu, B. Wang and X. Li, *J. Hazard. Mater.*, 2009, **164**, 1098–1104.

50 G. Bascialla and A. E. Regazzoni, *Colloids Surf., A*, 2008, **328**, 34–39.

51 N. Drici Setti, N. Jouini and Z. Derriche, *J. Phys. Chem. Solids*, 2010, **71**, 556–559.

52 A. R. Auxilio, P. C. Andrews, P. C. Junk, L. Spiccia, D. Neumann, W. Raverty and N. Vanderhoek, *Polyhedron*, 2007, **26**, 3479–3490.

53 R. M. M. dos Santos, R. G. L. Gonçalves, V. R. L. Constantino, L. M. da Costa, L. H. M. da Silva, J. Tronto and F. G. Pinto, *Appl. Clay Sci.*, 2013, **80–81**, 189–195.

54 R. r. Shan, L. g. Yan, Y. m. Yang, K. Yang, S. j. Yu, H. q. Yu, B. c. Zhu and B. Du, *J. Ind. Eng. Chem.*, 2015, **21**, 561–568.

55 M. Mustapha Bouhent, Z. Derriche, R. Denoyel, V. Prevot and C. Forano, *J. Solid State Chem.*, 2011, **184**, 1016–1024.

56 M. Bouraada, F. Belhalfaoui, M. S. Ouali and L. C. de Menorval, *J. Hazard. Mater.*, 2009, **163**, 463–467.

57 K. Nejati, Z. Rezvani, M. Mansurfar, A. Mirzaee and M. Mahkam, *Z. Anorg. Allg. Chem.*, 2011, **637**, 1573–1579.

58 H. Zaghouane-Boudiaf, M. Boutahala and L. Arab, *Chem. Eng. J.*, 2012, **187**, 142–149.

59 F. P. de Sá, B. N. Cunha and L. M. Nunes, *Chem. Eng. J.*, 2013, **215–216**, 122–127.

60 F. B. Saiah, B. L. Su and N. Bettahar, *J. Hazard. Mater.*, 2009, **165**, 206–217.

61 C. Zhang, S. Yang, H. Chen, H. He and C. Sun, *Appl. Surf. Sci.*, 2014, **301**, 329–337.

62 C. L. Guoqing Zhang, J. Zhao, J. Zhi Zhou, G. Qian, J. Liu and Y. Wu, *J. Water Sustainability*, 2012, **2**, 25–34.

63 A. Guzmán-Vargas, E. Lima, G. A. Uriostegui-Ortega, M. A. Oliver-Tolentino and E. E. Rodríguez, *Appl. Surf. Sci.*, 2016, **363**, 372–380.

64 Y. Lin, Z. Zeng, J. Zhu, Y. Wei, S. Chen, X. Yuan and L. Liu, *Mater. Lett.*, 2015, **156**, 169–172.

65 T. Xue, Y. Gao, Z. Zhang, A. Umar, X. Yan, X. Zhang, Z. Guo and Q. Wang, *J. Alloys Compd.*, 2014, **587**, 99–104.

66 R. Marangoni, M. Bouhent, C. Taviot-Gueho, F. Wypych and F. Leroux, *J. Colloid Interface Sci.*, 2009, **333**, 120–127.

67 K. Morimoto, K. Tamura, N. Iyi, J. Ye and H. Yamada, *J. Phys. Chem. Solids*, 2011, **72**, 1037–1045.

68 Y.-M. Zheng, N. Li and W.-D. Zhang, *Colloids Surf., A*, 2012, **415**, 195–201.

69 B. Bi, L. Xu, B. Xu and X. Liu, *Appl. Clay Sci.*, 2011, **54**, 242–247.

70 D. Chen, Y. Li, J. Zhang, W. Li, J. Zhou, L. Shao and G. Qian, *J. Hazard. Mater.*, 2012, **243**, 152–160.

71 D. Chen, Y. Li, J. Zhang, J.-z. Zhou, Y. Guo and H. Liu, *Chem. Eng. J.*, 2012, **185–186**, 120–126.

72 L. Nong, C. Xiao and W. Jiang, *Korean J. Chem. Eng.*, 2011, **28**, 933–938.

73 Q. Zhou, F. Chen, W. Wu, R. Bu, W. Li and F. Yang, *Chem. Eng. J.*, 2016, **285**, 198–206.

74 Y. P. Wei, D. Q. Wei and H. W. Gao, *Chem. Eng. J.*, 2011, **172**, 872–878.

75 Y. Li, H. Y. Bi, Y. S. Jin and X. Q. Shi, *RSC Adv.*, 2014, **4**, 58307–58314.

76 M. Bouraada, M. Lafjah, M. S. Ouali and L. C. de Menorval, *J. Hazard. Mater.*, 2008, **153**, 911–918.

77 P. Wu, T. Wu, W. He, L. Sun, Y. Li and D. Sun, *Colloids Surf., A*, 2013, **436**, 726–731.

78 C. Peng, J. Dai, J. Yu and J. Yin, *AIP Adv.*, 2015, **5**, 057138.

79 N. Benselka-Hadj Abdelkader, A. Bentouami, Z. Derriche, N. Bettahar and L. C. de Ménorval, *Chem. Eng. J.*, 2011, **169**, 231–238.

80 A. Auxilio, P. Andrews, P. Junk and L. Spiccia, *Dyes Pigm.*, 2009, **81**, 103–112.

81 E. Géraud, M. Bouhent, Z. Derriche, F. Leroux, V. Prévot and C. Forano, *J. Phys. Chem. Solids*, 2007, **68**, 818–823.

82 J. Orthman, H. Y. Zhu and G. Q. Lu, *Sep. Purif. Technol.*, 2003, **31**, 53–59.

83 D. D. Asouhidou, K. S. Triantafyllidis, N. K. Lazaridis and K. A. Matis, *J. Chem. Technol. Biotechnol.*, 2012, **87**, 575–582.

84 D. S. Tong, M. Liu, L. Li, C. X. Lin, W. H. Yu, Z. P. Xu and C. H. Zhou, *Appl. Clay Sci.*, 2012, **70**, 1–7.

85 R. Extremera, I. Pavlovic, M. R. Pérez and C. Barriga, *Chem. Eng. J.*, 2012, **213**, 392–400.

86 M. N. Pahalagedara, M. Samaraweera, S. Dharmarathna, C.-H. Kuo, L. R. Pahalagedara, J. A. Gascón and S. L. Suib, *J. Phys. Chem. C*, 2014, **118**, 17801–17809.

87 Z. Li, B. Yang, S. Zhang, B. Wang and B. Xue, *J. Mater. Chem. A*, 2014, **2**, 10202.

88 Z. M. Ni, S. J. Xia, L. G. Wang, F. F. Xing and G. X. Pan, *J. Colloid Interface Sci.*, 2007, **316**, 284–291.

89 Y. X. Zhang, X. D. Hao, T. Wang, Y. X. Meng and X. Han, *Dalton Trans.*, 2014, **43**, 6667–6676.

90 Y. X. Zhang, X. D. Hao, M. Kuang, H. Zhao and Z. Q. Wen, *Appl. Surf. Sci.*, 2013, **283**, 505–512.

91 Z. Yang, S. Ji, W. Gao, C. Zhang, L. Ren, W. W. Tjiu, Z. Zhang, J. Pan and T. Liu, *J. Colloid Interface Sci.*, 2013, **408**, 25–32.

92 S. A. Dhahir, E. Abdul-Hussein and N. Faraj, *Eur. Chem. Bull.*, 2013, **2**, 866–872.

93 Y. You, G. F. Vance and H. Zhao, *Appl. Clay Sci.*, 2001, **20**, 13–25.

94 Y. Yao, B. Gao, M. Inyang, A. R. Zimmerman, X. Cao, P. Pullammanappallil and L. Yang, *J. Hazard. Mater.*, 2011, **190**, 501–507.

95 I. M. Ahmed and M. S. Gasser, *Appl. Surf. Sci.*, 2012, **259**, 650–656.

96 X. Liang, Y. Zang, Y. Xu, X. Tan, W. Hou, L. Wang and Y. Sun, *Colloids Surf., A*, 2013, **433**, 122–131.

97 N. K. Lazaridis, T. D. Karapantsios and D. Georgantas, *Water Res.*, 2003, **37**, 3023–3033.

98 L. Sun, S. Wan and W. Luo, *Bioresour. Technol.*, 2013, **140**, 406–413.

99 T. W. Panpan Wua, W. Hea, L. Suna, Y. Lia and D. Sun, *Colloids Surf., A*, 2013, **436**, 726–731.

This journal is © The Royal Society of Chemistry 2016

100 F. Zhou, R. Shi and Y. Zhu, *J. Mol. Catal. A: Chem.*, 2011, **340**, 77–82.

101 M. A. M. Salleh, D. K. Mahmoud, W. A. W. A. Karim and A. Idris, *Desalination*, 2011, **280**, 1–13.

102 R. Hao, X. Xiao, X. Zuo, J. Nan and W. Zhang, *J. Hazard. Mater.*, 2012, **209–210**, 137–145.

103 R. Liikanen, J. Yli-Kuivila, J. Tenhunen and R. Laukkanen, *Desalination*, 2006, **201**, 58–70.

104 H. Abdolmohammad-Zadeh, E. Ghorbani and Z. Talleb, *J. Iran. Chem. Soc.*, 2013, **10**, 1103–1112.

105 S. Netpradit, P. Thiravetyan and S. Towprayoon, *J. Colloid Interface Sci.*, 2004, **270**, 255–261.

106 P. Janoš, H. Buchtová and M. Rýznarová, *Water Res.*, 2003, **37**, 4938–4944.

107 A. S. Özcan and A. Özcan, *J. Colloid Interface Sci.*, 2004, **276**, 39–46.

108 S. Wang and Z. H. Zhu, *J. Hazard. Mater.*, 2006, **136**, 946–952.

109 P. C. A. Anthony, R. Auxilio, P. C. Junk and L. Spiccia, *Aust. J. Chem.*, 2010, **63**, 83–91.

110 S. Yuan, S. Li, Q. Zhang and H. Wang, *Colloids Surf., A*, 2009, **348**, 76–81.

111 Y. Zhi, Y. Li, Q. Zhang and H. Wang, *Langmuir*, 2010, **26**, 15546–15553.

112 X.-L. Wu, L. Wang, C.-L. Chen, A.-W. Xu and X.-K. Wang, *J. Mater. Chem.*, 2011, **21**, 17353–17359.

113 T. Wen, X. Wu, X. Tan, X. Wang and A. Xu, *ACS Appl. Mater. Interfaces*, 2013, **5**, 3304–3311.

114 X. Yuan, Y. Wang, J. Wang, C. Zhou, Q. Tang and X. Rao, *Chem. Eng. J.*, 2013, **221**, 204–213.

115 J. Inacio, C. Taviot-Gueho, C. Forano and J. Besse, *Appl. Clay Sci.*, 2001, **18**, 255–264.

116 D. L. Sparks, *Geoderma*, 2001, **100**, 303–319.

117 L. Xiao, W. Ma, M. Han and Z. Cheng, *J. Hazard. Mater.*, 2011, **186**, 690–698.

118 S. Mandal, V. S. Patil and S. Mayadevi, *Microporous Mesoporous Mater.*, 2012, **158**, 241–246.

119 P. Zhang, G. Qian, H. Shi, X. Ruan, J. Yang and R. L. Frost, *J. Colloid Interface Sci.*, 2012, **365**, 110–116.

120 T. Kameda, T. Yoshioka, T. Mitsuhashi, M. Uchida and A. Okuwaki, *Water Res.*, 2003, **37**, 4045–4050.

121 N. K. Lazaridis, *Water, Air, Soil Pollut.*, 2003, **146**, 127–139.

122 M. Ulibarri, I. Pavlovic, M. Hermosin and J. Cornejo, *Appl. Clay Sci.*, 1995, **10**, 131–145.

123 X. Liu, X. Zhao, Y. Zhu and F. Zhang, *Appl. Catal., B*, 2013, **140–141**, 241–248.

124 P. Roy Chowdhury and K. G. Bhattacharyya, *Dalton Trans.*, 2015, **44**, 6809–6824.

125 K. Parida, L. Mohapatra and N. Baliarsingh, *J. Phys. Chem. C*, 2012, **116**, 22417–22424.

126 R. Kun, M. Balázs and I. Dékány, *Colloids Surf., A*, 2005, **265**, 155–162.

127 S. J. Xia, F. X. Liu, Z. M. Ni, J. L. Xue and P. P. Qian, *J. Colloid Interface Sci.*, 2013, **405**, 195–200.

128 M. Shao, J. Han, M. Wei, D. G. Evans and X. Duan, *Chem. Eng. J.*, 2011, **168**, 519–524.

129 L. Mohapatra and K. M. Parida, *Sep. Purif. Technol.*, 2012, **91**, 73–80.

130 K. M. Parida and L. Mohapatra, *Chem. Eng. J.*, 2012, **179**, 131–139.

131 X. Xu, R. Lu, X. Zhao, Y. Zhu, S. Xu and F. Zhang, *Appl. Catal., B*, 2012, **125**, 11–20.

132 G. Carja, E. Husanu, C. Gherasim and H. Iovu, *Appl. Catal., B*, 2011, **107**, 253–259.

133 J. H. Xin Shu and D. Chen, *J. Phys. Chem. C*, 2008, **112**, 4151–4158.

134 E. M. Seftel, E. Popovici, M. Mertens, K. D. Witte, G. V. Tendeloo, P. Cool and E. F. Vansant, *Microporous Mesoporous Mater.*, 2008, **113**, 296–304.

135 R. Huo, Y. Kuang, Z. Zhao, F. Zhang and S. Xu, *J. Colloid Interface Sci.*, 2013, **407**, 17–21.

136 L. Huang, S. Chu, J. Wang, F. Kong, L. Luo, Y. Wang and Z. Zou, *Catal. Today*, 2013, **212**, 81–88.

137 B. Benalioua, M. Mansour, A. Bentouami, B. Boury and H. Elandaloussi el, *J. Hazard. Mater.*, 2015, **288**, 158–167.

138 F. Khodam, Z. Rezvani and A. R. Amani-Ghadim, *RSC Adv.*, 2015, **5**, 19675–19685.

139 Y. F. Zhao, M. Wei, J. Lu, Z. L. Wang and X. Duan, *Nano*, 2009, **3**, 4009–4016.

140 R. K. Sahu, B. S. Mohanta and N. N. Das, *J. Phys. Chem. Solids*, 2013, **74**, 1263–1270.

141 Z. Huang, P. Wu, B. Gong, Y. Fang and N. Zhu, *J. Mater. Chem. A*, 2014, **2**, 5534.

142 X. Wang, P. Wu, Y. Lu, Z. Huang, N. Zhu, C. Lin and Z. Dang, *Sep. Purif. Technol.*, 2014, **132**, 195–205.

143 E. M. Seftel, M. Mertens and P. Cool, *Appl. Catal., B*, 2013, **134–135**, 274–285.

144 Z. Bouberka, K. A. Benabbou, A. Khenifi and U. Maschke, *J. Photochem. Photobiol., A*, 2014, **275**, 21–29.

145 Y. Zhou, W. Hu, J. Yu and F. Jiao, *React. Kinet., Mech. Catal.*, 2015, **115**, 581–596.

146 Y. L. Sujun Yuan, Q. Zhang and H. Wang, *Res. Chem. Intermed.*, 2009, **35**, 685–692.

147 Y. Zhou, L. Shuai, X. Jiang, F. Jiao and J. Yu, *Adv. Powder Technol.*, 2015, **26**, 439–447.

148 E. Dvininov, M. Ignat, P. Barvinschi, M. A. Smithers and E. Popovici, *J. Hazard. Mater.*, 2010, **177**, 150–158.

149 H. Fan, J. Zhu, J. Sun, S. Zhang and S. Ai, *Chemistry*, 2013, **19**, 2523–2530.

150 Y. Ao, D. Wang, P. Wang, C. Wang, J. Hou and J. Qian, *RSC Adv.*, 2015, **5**, 54613–54621.

151 R. Lu, X. Xu, J. Chang, Y. Zhu, S. Xu and F. Zhang, *Appl. Catal., B*, 2012, **111–112**, 389–396.

152 K. M. Parida, N. Baliarsingh, B. S. Patra and J. Das, *J. Mol. Catal. A: Chem.*, 2007, **267**, 202–208.

153 L. Mohapatra, K. Parida and M. Satpathy, *J. Phys. Chem. C*, 2012, **116**, 13063–13070.

154 S. j. Xia, X. b. Zhou, W. Shi, G. x. Pan and Z. m. Ni, *J. Mol. Catal. A: Chem.*, 2014, **392**, 270–277.

155 M. A. Carreon, S. Y. Choi, M. Mamak, N. Chopra and G. A. Ozin, *J. Mater. Chem.*, 2007, **17**, 82–89.

156 S. Y. Chae, M. K. Park, S. K. Lee, T. Y. Kim, S. K. Kim and W. I. Lee, *Chem. Mater.*, 2003, **15**, 3326–3331.

157 C. u. G. Silva, Y. s. Bouizi, V. Fornés and H. García, *J. Am. Chem. Soc.*, 2009, **131**, 13833–13839.

158 G. K. Zhang, X. M. Ding, F. S. He, X. Y. Yu, J. Zhou, Y. J. Hu and J. W. Xie, *Langmuir*, 2008, **24**, 1026–1030.

159 C. Ooka, H. Yoshida, K. Suzuki and T. Hattori, *Microporous Mesoporous Mater.*, 2004, **67**, 143–150.

160 E. Dvininov, M. Ignat, P. Barvinschi, M. A. Smithers and E. Popovici, *J. Hazard. Mater.*, 2010, **177**, 150–158.

161 B. H. Lee, S. S. Hong, K. H. Lee and Y. D. Kim, *J. Alloys Compd.*, 2004, **385**, 264–268.

162 S. P. Paredes, M. A. Valenzuela, G. Fetter and S. O. Flores, *J. Phys. Chem. Solids*, 2011, **72**, 914–919.

163 K. Lv, J. Yu, K. Deng, X. Li and M. Li, *J. Phys. Chem. Solids*, 2010, **71**, 519–522.

164 H. Fu, C. Pan, W. Yao and Y. Zhu, *J. Phys. Chem. B*, 2005, **109**, 22432–22439.

165 T. Kameda, S. Sato and T. Yoshioka, *J. Environ. Sci. Health, Part A: Toxic/Hazard. Subst. Environ. Eng.*, 2012, **47**, 2035–2039.

166 M. Z. b. Hussein, A. H. Yahaya and L. M. Ping, *Dyes Pigm.*, 2004, **63**, 135–140.